Investigations on Quantitative Phase Imaging in Biological Samples

Praveebalaji.R

A Dissertation Submitted to
Indian Institute of Technology Hyderabad
In Partial Fulfillment of the Requirements for
The Degree of Master of Technology

Department of Biomedical Engineering

June, 2017

Declaration

I declare that this written submission represents my ideas in my own words, and where others' ideas or words have been included, I have adequately cited and referenced the original sources. I also declare that I have adhered to all principles of academic honesty and integrity and have not misrepresented or fabricated or falsified any idea/data/fact/source in my submission. I understand that any violation of the above will be a cause for disciplinary action by the Institute and can also evoke penal action from the sources that have thus not been properly cited, or from whom proper permission has not been taken when needed.

R.Praveenbalaji

(Signature)

Praveenbalaji.R

(Student Name)

BM15MTECH11010

(Roll No)

Approval Sheet

This thesis entitled "Investigation on Quantitative Phase Imaging in Biological Samples" by Praveenbalaji.R is approved for the degree of Master of Technology from IIT Hyderabad.

R. Aravind

Dr. Aravind kumar Rengan
(Examiner1)

Dr. Renu John
(Supervisor)

Vandana Sharma

Dr. Vandana Sharma
(Examiner2)

Acknowledgements

Since I started my masters, there have been challenges in both academic and personal aspects of my life I am happy to see that in the end I was able to combine both the aspects and accomplish this goal. This accomplishment would not have been possible without the support of many people who always stood by me, some of them here and others in distance.

First, I would like to thank my supervisor, Dr. Renu John, Head of the Department and Associate Professor, Department of Biomedical Engineering, Indian Institute of Technology Hyderabad for his immense support and excellent guidance in carrying out this work. His invaluable suggestion and continuous encouragement served as a motivation in exploring new horizons in both academics and personal aspects of my life.

I would also like to thank Dr. Wataru Watanabe, Assistant professor, Department of Electrical engineering, Ritsumeikan University ,Japan for his support during my internship period.

I am also grateful to Mr. Hanu Phani Ram for sharing his knowledge and expertise with me.

I would also like to express my gratitude to Mr. Gaurav Versain Kapoor for the moral support and timely help whenever I am in need.

Finally, I would like to thank my parents for their constant love and motivation throughout my course of study at IIT Hyderabad.

.

Dedicated to

My guide

Abstract

In this thesis, titled “Investigations on Quantitative Phase imaging in Biological Samples” two works have been reported. In the first work, we demonstrate a novel method to retrieve the information behind the scattering media by employing the statistical properties of speckle. This work is carried out by measuring the complex coherence function of spatially fluctuating speckle using the intensity correlation and speckle holographic principle. Experimental studies to recover the information behind the multiple scattering media is practically demonstrated and the information is recovered. The proposed method finds numerous applications in optical imaging especially in biomedical imaging. In the second work, a novel coded illumination microscope technique, which enables the successive acquisition of bright field, dark field and phase contrast images, is demonstrated. A simple experimental geometry for the multi modal imaging system along with an algorithm to retrieve the quantitative phase information form the phase contrast images is devised and the results are demonstrated for various phase objects.

Nomenclature

λ	Wavelength
I	Intensity
c	Speed of light
t	Transmission function
E_o	Electric field distribution
ΔI_o	Object intensity
BS	Beam splitter
MO	Microscope objective
$P(\theta)$	Probability of finding facet
k	Wave number
μ_a	Complex coherence factor
ς_1	Power spectral density
K_o	Covariance function
C	Complex coherence function
$Nd{:}YAG$	Neodymium-doped Yttrium Aluminium Garnet
CCD	Charge coupled device
NA	Numerical aperture
FOV	Field of view

List of Figures

Contents

Chapter 1

Introduction

1.1 Motivation

Imaging techniques employing visible light have been a standard research tool for centuries: vision is usually our most developed sense, and thus the visual inspection of a specimen has always been a scientist's first choice. The development of lenses, telescopes, and microscopes has helped us visually explore large or small worlds previously not accessible. Unlike conventional imaging techniques that use ionizing radiation for investigations, optical imaging makes use of the visible and infrared spectrum of electromagnetic spectrum for investigation. The application of optical imaging is growing in the field of biomedical studies and life sciences due to its non-invasive and non-ionizing nature. In spite of several advancements and development of various techniques, imaging through a highly scattering media such as biological tissues is one of the long lasting problem and a prime challenge in optical imaging.

The coherent light scattering from the highly scattering media results in the formation of speckle patterns. These speckle patterns can be utilized for extracting the information about the illuminated surface that generates it. From the perspective of statistical optics in coherence theory of light the far field speckles can be related to the incoherent course structure through Van Cittert-Zernike theorem i.e. two-point correlation between the two points at a far field is related to the spatially fluctuating random object field by Fourier transform. By combining the statistical properties of light mainly auto correlation of intensity and the principle of holography a new method can be developed to image through the scattering media. As the human tissue is a highly scattering media, the role of complex correlation in biomedical imaging is of uttermost importance with its applicability in various research areas of biomedical sciences.

Optical microscopy is one of the oldest scientific instruments of the sciences and continues to be an essential tool for researchers, clinicians and engineers across many disciplines. Continuous advancements in microscopy over the past decades have introduced many new imaging modalities. However, bright field, dark field and phase contrast are the most common label free contrast modes used in microscopy. Bright field imaging is most suitable for observing samples with strong absorption. Dark field imaging provides good contrast for sub resolution features. Phase contrast imaging is used for unstained and transparent biological samples allowing visualization of shape and density variations. Since each of bright field, dark field and phase contrast imaging provides complimentary information about a sample, it is often desired to use multiple methods at once. However, in traditional microscopes each contrast modes relies on a different optical hardware configuration, requiring inserts at the condenser aperture, polarization components and specialized objectives.

The diverse imaging capability in a single microscopic hardware platform is achieved by replacing the conventional Kohler illumination source by LED array at the source plane. The three contrast modes is achieved by sequentially illuminating the appropriate patterns in the LED array. Beyond the contrast modes, a novel algorithm for quantitative phase reconstruction is also devised. Due to the simplicity of the LED array microscope setup and diverse range of imaging capabilities, the development of this multi-contrast microscopic scheme finds variety of applications in biomedical sciences thus bringing down the cost of conventional microscopes.

1.2 Scope of the thesis

The objective of the primary work is to develop an optical imaging technique for imaging through scattering media by employing the speckle statistics approach. This is carried out my measuring the second order correlation i.e. complex correlation function of a spatially fluctuating speckle at far field using the principles of speckle holography.

The objective of the secondary work is to develop a microscopic hardware platform capable of acquiring bright field, dark field and phase contrast images without the requirement of distinct optical elements. This is achieved by replacing Kohler illumination unit of conventional microscope with programmable LED array source.

.

1.3 Organization of the thesis

Chapter 2 of this thesis gives an overview of holography imaging and its applications in optical imaging. The chapter gives an insight to basic understanding of different holographic imaging techniques.

Chapter 3 of the thesis discusses the effect of coherent light passing through the scattering media. Along with it the properties of first order and second order speckle statistics is discussed. In addition, the experimental setups for imaging through the scattering media and algorithm for retrieval of information from the speckle field is discussed and the results are demonstrated.

Chapter 4 of the thesis discusses about the basic principle of multi contrast microscopy and the advantages of using LED arrays as the light source. In addition, a novel quantitative phase reconstruction technique and the experimental setup for multi contrast microscopy is discussed and results for different biological samples are demonstrated.

Chapter 5 of the thesis gives the summary and future work of the given project.

.

Chapter 2

Holography Imaging

2.1 Basics of Holography Imaging

In 1948, Dennis Gabor introduced " A new microscopic principle"[1], which he termed holography from the Greek words 'halos' which means complete and 'graphein' which means to write. This name was coined to indicate that the method records the entire field information (i.e. amplitude and phase) not just the usual intensity. In 1971, Dennis Gabor was awarded the Nobel Prize in Physics "for his invention and development of the holographic method".

The holography involves two major steps recording the hologram and reconstructing the hologram. As the recording media responds only to the intensity of light, it is not possible to detect the complete information i.e. amplitude and phase of the object [2]. In order to record the amplitude and phase of the object, the interferometric technique is applied in which the coherent reference wave front will add with unknown object wave front and generates an interference pattern which can be recorded on the recording media. This interference pattern recorded is called hologram and it contains the complete information of the object.

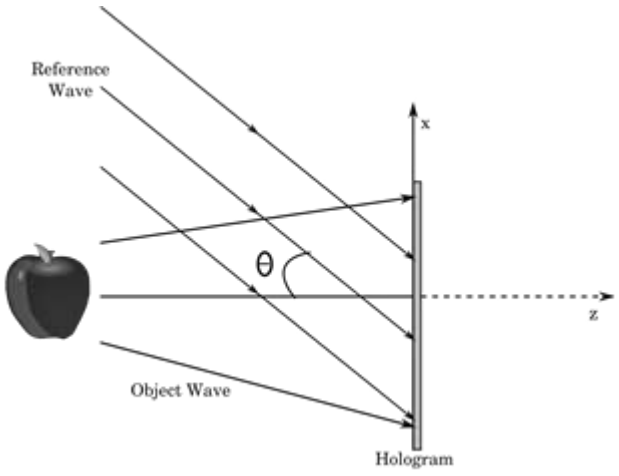

Figure 2.1: Optical system for recording a hologram.

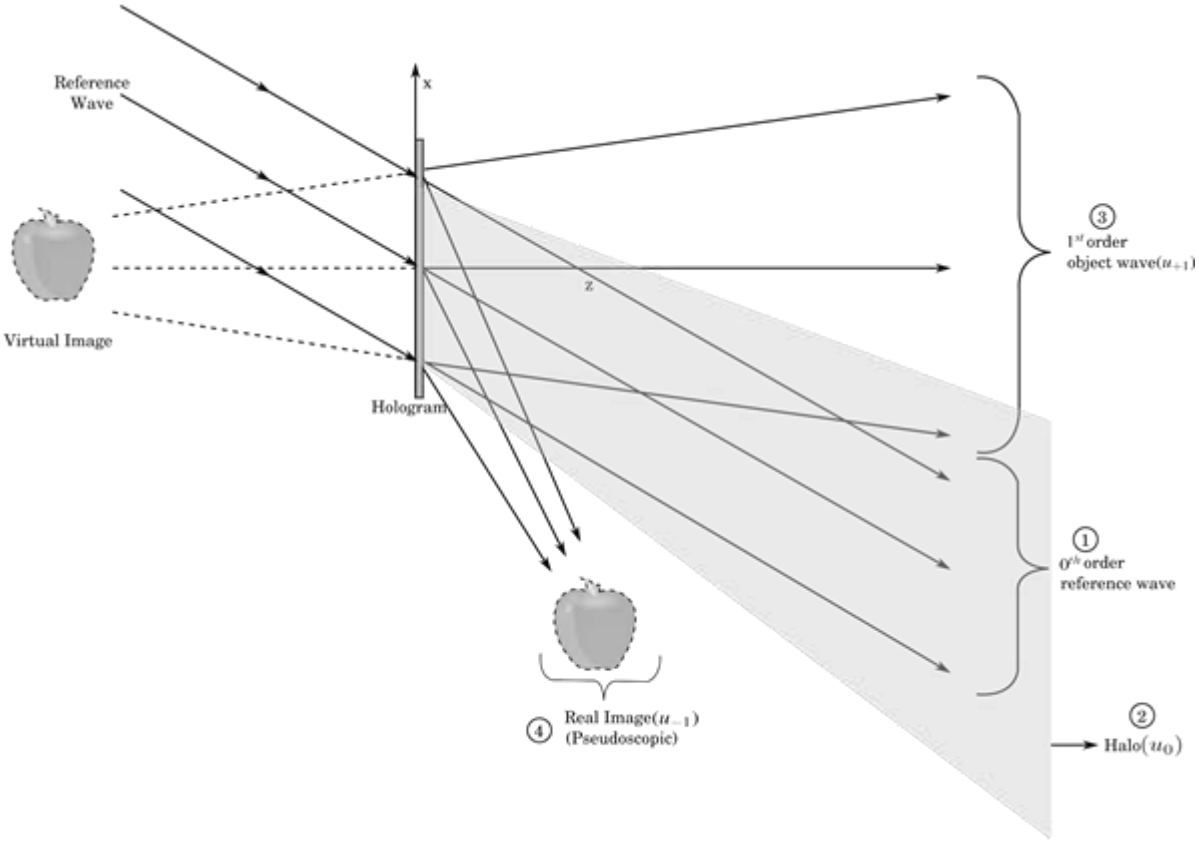

Figure 2.2: Optical system for reconstructing a hologram.

2.1.1 Gabor/Inline Hologram

In Inline holography, the object is illuminated by a collimated beam of monochromatic light along an axis normal to the photographic plate. The light incident on the photographic plate then contains two components. The first is the directly transmitted wave, which is a plane wave whose amplitude and phase do not vary across the photographic plate. The second is a weak scattered wave, which emanates from the object. Both these waves superimpose on the photographic plate-giving rise to fringe pattern, which is the hologram.

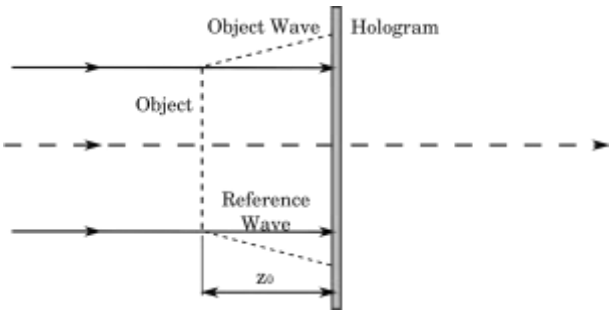

Figure 2.3: Gabor/Inline hologram recording.

The reference wave can be expressed as

$$A = A(x, y) \tag{2.1}$$

The scattered wave emanating from the object can be expressed as

$$a(x, y) = |a(x, y)| e^{i\phi(x,y)} \tag{2.2}$$

Where $|a(x, y)|$ represents the amplitude and $\phi(x, y)$ phase part of the object

The intensity of the interference pattern recorded at recording medium can be expressed as

$$I(x, y) = |A|^2 + |a(x, y)|^2 + A^* a(x, y) + A a^*(x, y) \tag{2.3}$$

From the Equation 2.3, it seems that the complete details of object have been encoded in interference pattern of waves. Usually recording of the interference pattern has been done with photographic plate. However new digital techniques are available to detect the intensity of light, which we will explore later in digital holography technique. Once the hologram of the object is recorded it is necessary to reconstruct it, which is the second step of holography. The developed transparency of the hologram is directly proportional to the exposure and is given by

$$t_A(x, y) = t_b + \beta(|a|^2 + A^* a + A a^*) \tag{2.4}$$

Where t_A represents amplitude transmittance of hologram, t_b represents transparency corresponds to constant reference wave and β' represents transparency constant. If the transparency is illuminated by uniform coherent source same as that of plane reference *B*, one can recover complete information of complex object as given by the equation

$$B t_A = B t_b + \beta B |a(x, y)|^2 + \beta A^* B a(x, y) + \beta A B a^*(x, y) \tag{2.5}$$

In the above equation, the first term is spatially constant, the second term is termed as "object halo" and it is negligible as for a transparent object the un-scattered field is much stronger than the scattered field. The final two terms of the Equation 2.5 corresponds to a focused real image and an out of focus virtual image.

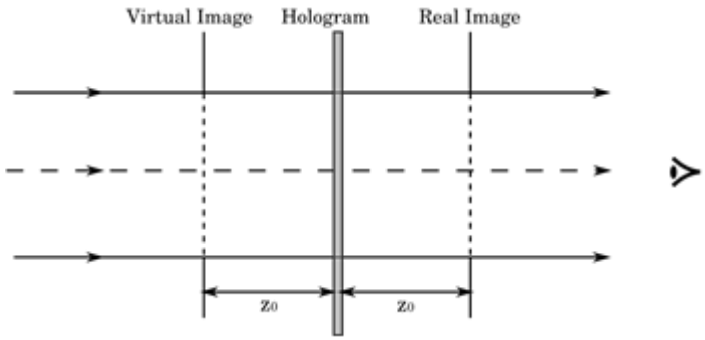

Figure 2.4: Gabor/Inline hologram reconstruction.

Reconstruction of the in-line hologram generates both virtual and real image of object simultaneously centered on hologram axis and these are called twin images. The formation of real and virtual images from Gabor inline hologram is shown in Figure 2.4. Generation of twin image is the main drawback of in line holography, which is eliminated by development of off-axis holography called Leith-Upatnieks Holography [3].

2.1.2 Leith-Upatnieks /Off-axis holography

Leith-Upatnieks developed and implemented a new modified technique to solve the twin image problem in holography [3]. The critical difference between inline and off-axis holography is that the reference beam is set at an angle to the object beam in off-axis holography. This angle off set adds a carrier frequency to the signal as long as this is sufficiently high, the twin image problem of inline holography can be avoided and the amplitude and phase of the light from the original object can be unambiguously reconstructed from hologram.

The recording arrangement for off-axis holography is shown in Figure 2.5. The reference beam is a collimated beam of uniform intensity, derived from the same source as that used to illuminate the object. The reference beam interfere with the collimated beam illuminating the object at a tilted angle normal to the recording plane.

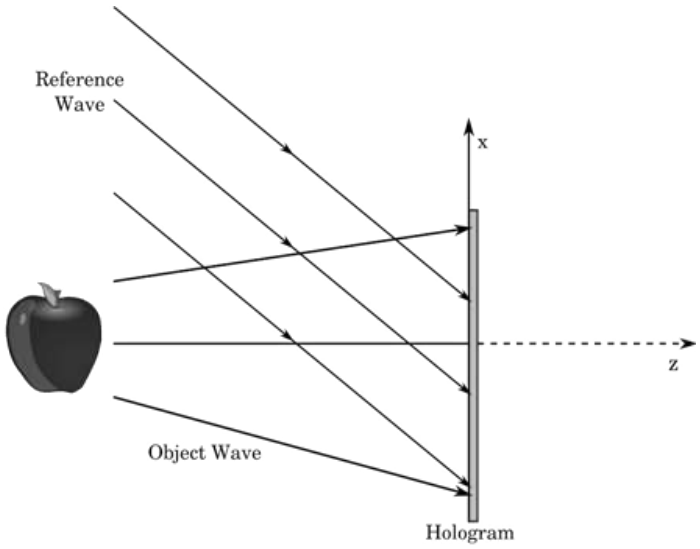

Figure 2.5: Leith-Upatnieks/Off-axis hologram recording.

The recorded field can be written as

$$U(x,y) = A\exp(-j2\pi\alpha y) + a(x,y) \qquad 2.6$$

Where α is the spatial frequency of reference wave which can be written as

$$\alpha = \frac{\sin 2\theta}{\lambda} \qquad 2.7$$

The intensity distribution at recording plane is expressed as

$$I(x,y) = |A|^2 + |a(x,y)|^2 + A^* a(x,y)\exp(j2\pi\alpha y) + A a^*(x,y)\exp(-j2\pi\alpha y) \qquad 2.8$$

The object wave $\boldsymbol{a}(x,y)$ can be expressed as

$$a(x,y) = |a(x,y)|\exp[j\Phi(x,y)] \qquad 2.9$$

Alternatively, the intensity distribution at recording plane can be expressed in term of amplitude and phase of the object as

$$I(x,y) = |A|^2 + |a(x,y)|^2 + 2|A||a(x,y)|\cos(2\pi\alpha y - \phi(x,y)) \qquad 2.10$$

From the above expression of intensity distribution, it is evident that a sufficient carrier frequency is required to separate twin images from the DC; if the spatial carrier frequency is sufficiently high, the object information can be recorded and reconstructed without any distortion.

The amplitude transparency after recording the hologram can be written as

$$t_A = t_b + \beta'\left(|a(x,y)|^2 + A^* a(x,y)\exp(j2\pi\alpha y) + Aa^*(x,y)\exp(-j2\pi\alpha y)\right) \quad 2.11$$

For easier description the above equation can be written as

$$t_1 = t_b \qquad t_2 = \beta'|a(x,y)|^2 \quad t_3 = \beta' A^* a(x,y)\exp(j2\pi\alpha y)$$

$$t_4 = \beta' Aa^*(x,y)\exp(-j2\pi\alpha y)$$

The object wave front is reconstructed by illuminating the transparency by uniform coherent source *B* same as that of the reference beam. The reconstruction of the object wave front is demonstrated in the Figure 2.6.

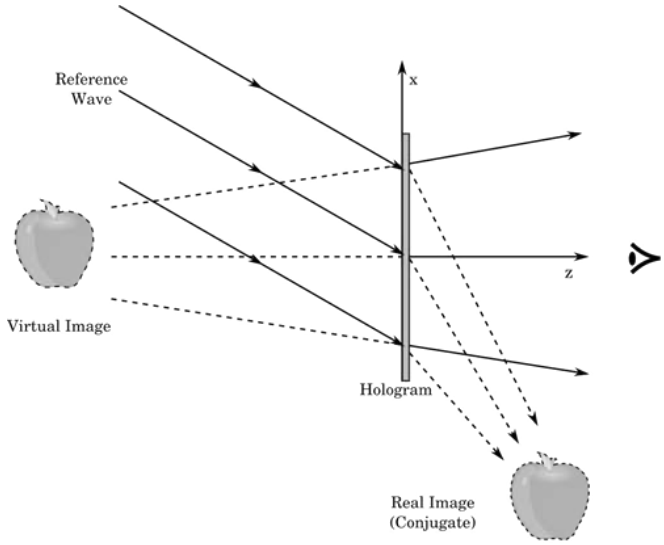

Figure 2.6: Leith-Upatnieks/Off-axis hologram reconstruction.

The reconstructed wave field can be expressed as

$$t_A = U_1 + U_2 + U_3 + U_4 \quad 2.12$$

Where

$$U_1 = t_b B \qquad U_2 = \beta' B|a(x,y)|^2 \quad U_3 = \beta' A^* Ba(x,y)\exp(j2\pi\alpha y)$$

$$U_4 = \beta' BAa^*(x,y)\exp(-j2\pi\alpha y)$$

The components U_1 and U_2 corresponds to direct attenuated transmitted light and spatially varying DC component from object respectively. While U_3 and U_4 gives virtual and real image angularly separated as shown in the Figure 2.6. The conventional process of holography using photographic plates is time consuming and cumbersome. The recent developments in the field of electronics and computers gave rise to a new paradigm of holography called digital holography, which we will discuss, in next section.

2.2 Digital Holography

Digital holography is a technique of recording the holograms with (Charge Coupled Devices CCD/ (Complementary Metal Oxide Semiconductors) CMOS and enables their subsequent reconstruction within the computers, thus avoiding the photographic process used in optical holography. In 1994, Schnars and Jueptner became the first scientists to use a CCD camera directly connected to a computer as the input in a holography setup [4]. Since then the development of digital holographic techniques and applications have been gaining pace more rapidly.

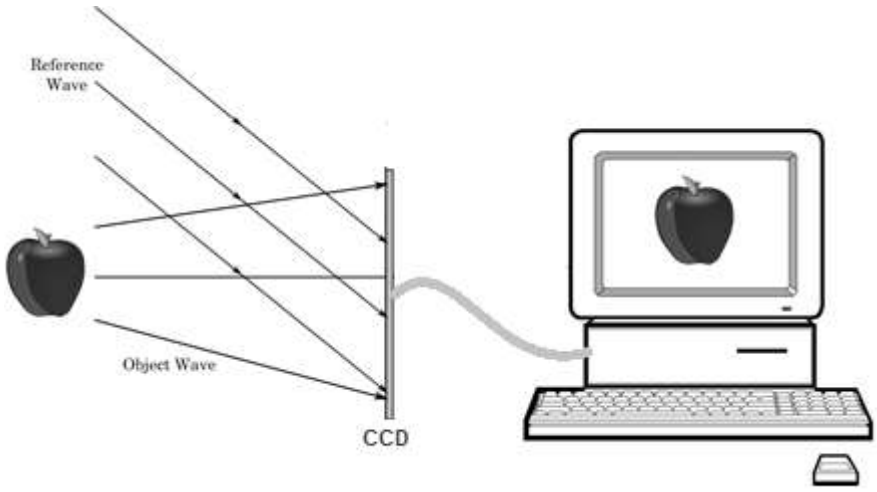

Figure 2.7: Digital holography recording and reconstruction.

Figure 2.7 shows the process in which the hologram is recorded optically, but a CCD is used for recording instead instead of photographic plate. The recorded hologram is then fed in to the computer and it is reconstructed on the computer by simulating the reference wave propagation.

The digital holographic imaging principles are highly useful in imaging through a random media and the method of speckle holography, which we will discuss, in the next chapter, is utilized in our imaging technique and has potential applications in biomedical research.

Chapter 3

Imaging through scattering media

3.1 Scattering and diffusion theory

First we introduce the basic terminology in scattering theory with emphasis on biological tissues and visible to near infrared (NIR) spectrum (400-1350nm). In this spectrum range most biological tissues are characterized by strong scattering and absorption [5]. Hence, it is considered as imaging window in biological samples.

The propagation of electromagnetic radiation in scattering media is characterized by different length scales, which are defined by:

- Scattering mean free path, defined as the average distance between two consecutive scattering events. In tissue, it is of the order of $0.1mm$ [6]. The scattering coefficient μs is defined as the inverse of the scattering mean free path.
- Mean absorption path, defined as the average distance a photon travels before it is absorbed in the medium. In tissue it can extend to $10 – 100mm$ [6]. The absorption coefficient μa is defined as the inverse of the mean absorption path.
- Mean free path (MFP), defined as the distance a photon travels before it is scattered or absorbed. The MFP is defined by its inverse — the transport coefficient μt , such that $\mu t = \mu a + \mu s$. In tissue usually $\mu s >> \mu a$ such that the mean free path is simply the scattering mean free path.
- Transport mean free path (TMFP), defined as the distance a photon propagates while it undergoes several scattering events and is still correlated to the original direction. Similarly, it is defined by the inverse $\mu' s$ such that $\mu' s = \mu s(1-g)$ where g is the anisotropy function which defines the degree of forward scattering, in tissue $g \sim 0.9$ [7].

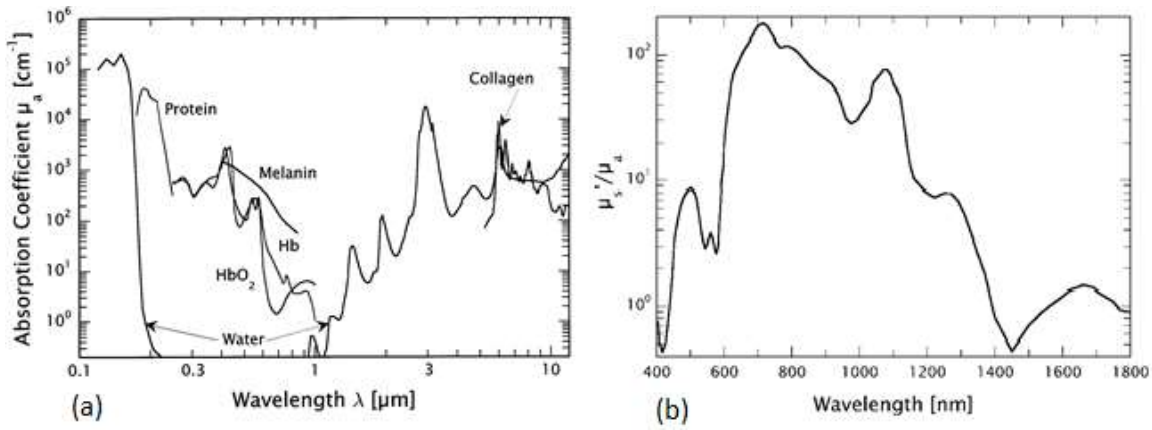

Figure 3.1: Absorption and Scattering in biological tissues (a) Absorption coefficient vs Optical wavelength in the range of 0.1-10 *μm*. (b) Scattering coefficient vs Optical wavelength in the range of 400-1800 *nm*. Scattering outside this is not characterized since it is dominated by absorption.

When a photon interact with scattering medium it can undergo several events

- Specular reflection – from the surface to medium
- Absorption – with in the medium
- Diffusion reflection – after going through one or more scattering events within media
- Direct transmission – no interaction within media
- Diffuse transmission- transmission through medium after going through one or more scattering events. These photons are usually divided in to

  -Snake photons, which undergo very little scatterings

  -Diffused photons, which go through significant amount of scattering

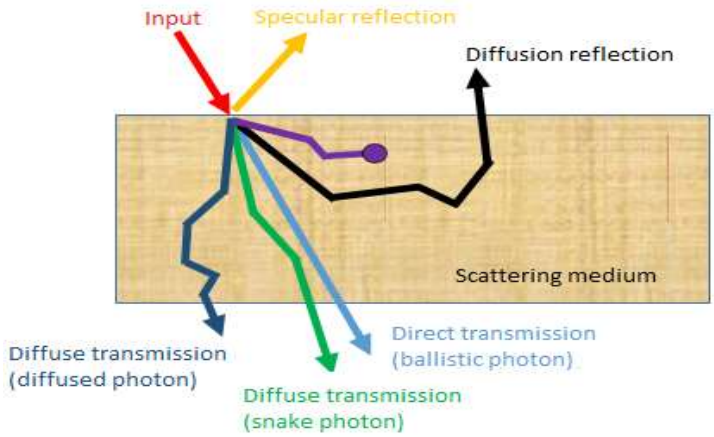

Figure 3.2: Different events a photon can undergo during transport in scattering media.

3.2 Coherent Scattering – Speckles

Speckles are random set of dark and bright spots formed when a coherent light is either reflected from a rough surface or propagates through a medium with random intensity fluctuations [8]. As in any interference pattern, the bright spots correspond to positions in space in which the scattered waves from the surface or by some particles inside the medium arrive in phase. On the other hand, the dark spots correspond to positions where destructive interference takes place because the scattered waves arrive out of phase.

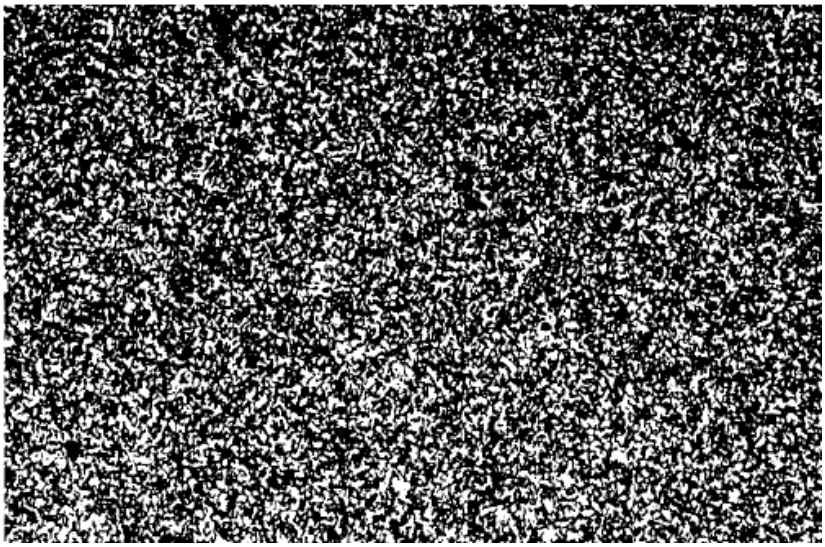

Figure 3.3: A laser speckle pattern.

According to the geometry involved in the formation of the speckles, they can be divided in two groups. The speckle pattern resulting from the back scattered light in the absence of a lens system when a coherent light illuminates a sample is known as objective speckles. In contrast, when the laser-illuminated sample is imaged with a sensor through a lens system the resulting speckles are known as subjective speckles. Due to the fact that the speckle patterns involved in this work are done using lenses, hereafter only subjective speckles will be considered.

Traditionally speckles are considered as an unwanted phenomenon because it corrupts the images obtained with coherent radiation [9.10]. However since the discovery that speckle encodes information about the surface, several applications based on the analysis of speckle pattern were found, some of which have evolved in current biomedical applications to track and measure blood flow [11].

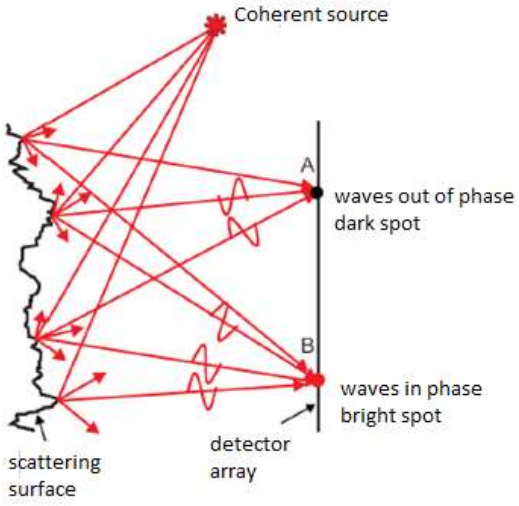

Figure 3.4: laser speckle formation.

3.3 Speckle Statistics

Speckles exhibit a spatial random intensity due to the random phases of the scattering waves interfering to form it. Hence, the proper approach to explain the speckle phenomena contemplates is the use of statistics. In this section, we will look into the first and second order speckle statistical properties. A brief introduction to first order properties will be presented followed by the second order speckle properties especially intensity correlation function which can be utilized for imaging through the turbid media.

3.3.1 First Order Speckle Statistics

The first order speckle statistics refers to the speckle statistics calculated at a single point in space and is capable of describing the fluctuations in the speckle pattern [14]. In order to calculate these values at a single detection point, scattered field probability distribution plays a vital role as by using them one can calculate the first order speckle statistics of the speckle pattern mainly mean value and variances [12].

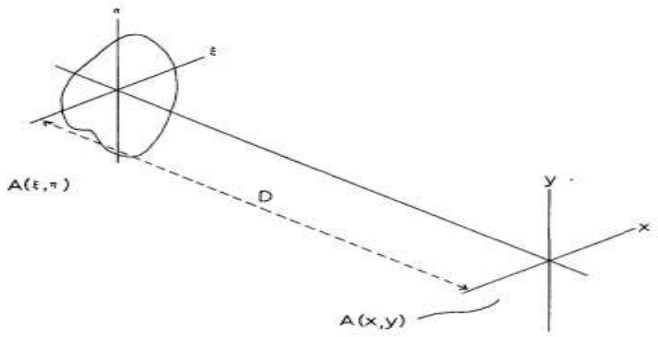

Figure 3.5: Formation of speckle pattern in Fraunhoffer plane.

Let a speckle pattern be formed from the coherent light in an observation plane as shown in the Figure 3.5.

We can write the complex amplitude of the scattered wave as suggested in [13] as

$$A(\xi,\eta)=\sum_{j=1}^{N} a_j e^{(ib_j)\delta(\xi-\xi_j)\delta(\eta-\eta_j)} \tag{3.1}$$

Where N is the number of stutterers, a_j is the modulus of the scattered wave due to scatterer, $\delta(\xi)\delta(\eta)$ is the two dimensional Dirac delta function, b_j is the phase of the wave.

Taking the Gaussian far field assumptions, the complex amplitude $A(x,y)$ can be written as

$$A(x,y)=\int_{-\infty}^{\infty}\int A(\xi,\eta)e^{\left[-\frac{2\pi i}{\lambda d}(x\xi+y\eta)\right]}d\xi d\eta \tag{3.2}$$

From Equation 3.10, 3.11 and by making use of Fourier transform we get

$$A(x,y)=\sum_{j=1}^{N} a_j e^{(ib_j)} e^{\left[-\frac{2\pi i}{\lambda d}(x\xi_j+y\eta_j)\right]} \tag{3.3}$$

Also, the probability density distributions of the scattered complex field amplitude have a Gaussian form which can be derived from central limit theorem [12]. The probability density of the field phase can be characterized by the uniform distribution and accordingly the probability density for developed speckles has a negative exponential form as shown below

$$p(I)=\frac{1}{\langle I\rangle}e^{-\left(\frac{1}{\langle I\rangle}\right)} \tag{3.4}$$

The above property can be manifested as the unit value of the speckle contrast, which can be written as follows

$$C=\frac{\sigma_I}{\langle I\rangle}=1 \tag{3.5}$$

The contrast is the ratio between the standard deviation and mean value of the speckle intensity fluctuations. Also, the relation between the developed speckle patterns for first and higher order statistical moments can be written as

$$\frac{\langle I\rangle}{\langle I_n\rangle}=n! \tag{3.6}$$

And can be easily calculated from the statistical moments as shown in Equation 3.7.

$$\left\langle I^n \right\rangle = \int_0^\infty I^n \rho(I) di \qquad 3.7$$

A scattering surface consisting of many equal sized facets produces non-Gaussian speckle distribution characterized by the dependency of second order normalized moment of intensity fluctuations upon the system parameters as shown in Equation 3.8.

$$\frac{\left\langle I^2 \right\rangle}{\left\langle I \right\rangle^2} = 2(1 - N^{-1}) + \left[\frac{k^2 \Psi^2}{4\pi P(\theta)} \right] N^{-1} \left\langle I^n \right\rangle = \int_0^\infty I^n \rho(I) di \qquad 3.8$$

In the above equation

k is the wave number of the light.

N is the number of facets within the area of illumination.

ψ is the radius.

$P(\theta)$ is the probability of finding the facet

If the speckle is fully developed, the first order statistics of the speckle fluctuations are completely non-dependent on the scattering object structural properties therefore they cannot be utilized for characterization of the scattering but they are enough to explain the brightness fluctuations. The speckle intensity statistics for a known illumination are the basis for several speckle technologies. The detailed study of first order speckle statistics can be found in [14] for better understanding. We now look into our main topic of interest i.e. the second order speckle statistics.

3.3.2 Second Order Speckle Statistics

The second order statistics of the scattered field describes the spatial structure of the field [14]. Let us consider a monochromatic light that is incident on a rough surface and the scattered field observed at some distance in the observation plane as shown in Figure 3.6.

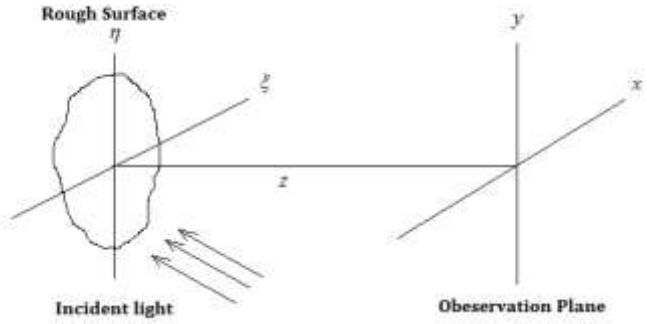

Figure 3.6: Free space propagation geometry for speckle formation.

The complex field $A(x, y)$, observed across the parallel plane with the (ξ, η) plane at a distance *z* from it, represents the speckle field of interest. The intensity distribution in the (x, y) plane can be represented as

$$I(x, y) = |A(x, y)|^2 \qquad 3.9$$

The autocorrelation function of the intensity distribution $I(x, y)$ at the observation plane (x, y) is given as [15]

$$R_I(x_1, y_1; x_2, y_2) = \langle I(x_1, y_1) I(x_2, y_2) \rangle \qquad 3.10$$

Where $\langle\ \rangle$ represents ensemble average over the randomly observed field. The width of autocorrelation provides estimate of size of the speckle.

To calculate autocorrelation function, we assumed that the scattering surface roughness is in the order of the wavelength of the illuminating light and randomly fluctuating field at the observation plane follow complex circular Gaussian characteristics. Corresponding to this field, the autocorrelation function of intensity can be written in term of the two point complex correlation of the random field as

$$W_A(x_1, y_1; x_2, y_2) = \langle A(x_1, y_1) A^*(x_2, y_2) \rangle \qquad 3.11$$

Where W refers to mutual intensity of the field in accordance with coherence theory.For circular complex Gaussian fields the relation between R_I and W expressed as

$$R_I(x_1, y_1; x_2, y_2) = \langle I(x_1, y_1) \rangle \langle I(x_2, y_2) \rangle + |W(x_1, y_1; x_2, y_2)|^2 \qquad 3.12$$

Here $W_A(x_1, y_1; x_1, y_1) = \langle I(x_1, y_1) \rangle$ represents the single point correlation and is nothing but the intensity at the point (x_1, y_1).

The calculation of mutual intensity in the observation plane (x, y) can be derived from Huygens – Fresnel principle expressed in Fresnel approximation as

$$A(x,y) = \frac{1}{\lambda z}\exp\left[\frac{-i\pi}{\lambda z}(x^2+y^2)\right]\iint_{\infty} A(\xi,\eta)\exp\left[\frac{-i\pi}{\lambda z}(\xi^2+\eta^2)\right]\exp\left[\frac{i2\pi}{\lambda z}(x\xi+y\eta)\right]d\xi d\eta \quad 3.13$$

Using equation, the two-point complex correlation function of field is written as

$$\begin{aligned} W_A(x_1,y_1;x_2,y_2) = & \\ & \frac{1}{\lambda^2 z^2}\exp\left[\frac{i\pi}{\lambda z}({x_1}^2-{x_2}^2+{y_1}^2-{y_2}^2)\right]\times \\ & \iint\iint_{\infty} W_\alpha(\xi_1,\eta_1;\xi_2,\eta_2)\times\exp\left[\frac{i\pi}{\lambda z}({x_1}^2-{x_2}^2+{y_1}^2-{y_2}^2)\right]\times \\ & \exp\left[\frac{i2\pi}{\lambda z}(x_1\xi_1+y_1\eta_1-x_2\xi_2-y_2\eta_2)\right]d\xi_1 d\eta_1 d\xi_2 d\eta_2 \end{aligned} \quad 3.14$$

As the microstructure of the scattering surface is assumed so fine to be unresolvable by a lens size of our observation region in the (x, y) plane. The curvature term of Equation 3.14 can be avoided using a Fourier transforming lens and detecting the scattered field at the far field. The mutual intensity at the scattering field is given by

$$W_\alpha(\xi_1,\eta_1;\xi_2,\eta_2) \cong kP(\xi_1,\eta_1)P^*(\xi_2,\eta_2)\delta(\xi_1-\xi_2,\eta_1-\eta_2) \quad 3.15$$

Where k proportionality constant, $P(\xi,\eta)$ amplitude distribution of incident on scatter and $\delta(\xi,\eta)$ two-dimensional deltas function.

The result of the simplification is

$$W_A(x_1,y_1;x_2,y_2) \cong \frac{k}{\lambda^2 z^2}\int\int_{-\infty}^{\infty}\left|P(\xi_1,\eta_1)\right|^2\exp\left\{\frac{i2\pi}{\lambda z}\left[\xi_1(x_1-x_2)+\eta_1(y_1-y_2)\right]\right\}d\xi_1 d\xi_2 \quad 3.16$$

This relation is extremely analogous to the *Van Cittert-Zernike theorem* of complex coherence theory.

The normalized version of mutual intensity known as complex coherence factor is defined by

$$\mu_A(x_1,y_1;x_2,y_2) = \frac{W_A(x_1,y_1;x_2,y_2)}{\left[W_A(x_1,y_1;x_1,y_1)W_A(x_2,y_2;x_2,y_2)\right]^{1/2}} \quad 3.17$$

Using Equation 3.16, the complex coherence takes the form

$$\mu_A(\Delta x,\Delta y)=\frac{\int\int_{-\infty}^{\infty}|P(\xi,\eta)|^2\exp\left[\frac{i2\pi}{\lambda z}(\xi\Delta x+\eta\Delta y)\right]d\xi d\eta}{\int\int_{-\infty}^{\infty}|P(\xi,\eta)|^2 d\xi d\eta} \qquad 3.18$$

The auto-correlation function of the speckle intensity assumes the form

$$R_I(\Delta x,\Delta y)=\langle I\rangle^2\left[1+|\mu_A(\Delta x,\Delta y)|^2\right] \qquad 3.19$$

$$=\langle I\rangle^2\left[1+\left|\frac{\int\int_{-\infty}^{\infty}|P(\xi,\eta)|^2\exp\left[\frac{i2\pi}{\lambda z}(\xi\Delta x+\eta\Delta y)\right]d\xi d\eta}{\int\int_{-\infty}^{\infty}|P(\xi,\eta)|^2 d\xi d\eta}\right|^2\right] \qquad 3.20$$

From the perspective of second order speckle statistics, Power spectral density of the intensity distribution $I(x,y)$ is an important quantity. The power spectral density $\varsigma_1(v_x,v_y)$ is given by the Fourier transform of auto correlation function. $R_f(\Delta x,\Delta y)$

Applying the Fourier transform to Equation 3.20 we can write power spectral density $\varsigma_1(v_x,v_y)$ as

$$\varsigma_I(v_X,v_y)=\langle I\rangle^2\left\{\delta(v_X+v_y)+\frac{\int\int_{-\infty}^{\infty}|P(\xi,\eta)|^2\left|P(\xi-\lambda z v_X,\eta-\lambda z v_y)\right|^2 d\xi d\eta}{\left[\int\int_{-\infty}^{\infty}|P(\xi,\eta)|^2 d\xi d\eta\right]^2}\right\} \qquad 3.21$$

The relation shows that the Power Spectral Density of speckle pattern consists of delta function at zero frequency i.e. at $v_X=0$ and $v_y=0$; and the spectrum having shape of normalized autocorrelation function of intensity distribution over the scatter.

3.4 Complex correlation measurement using two- point intensity correlation

Hanbury Brown and Twiss (HBT) introduced the concept of two-point intensity correlation in the 1950's for the measurement of angular size of distance star from independent detectors at different location by using classical approach for radiation field [16]. Usually the two-point intensity correlation is measured by utilizing the temporal averaging as a replacement of spatial averaging to time varying random field. In case of spatially varying

random field distribution originated from laser speckle having Gaussian statistics the two-point intensity correlation is measured by replacing ensemble averaging with the spatial averaging under the conditions of spatial ergodicity and stationarity. Here, a method to measure complex correlation function using the two-point intensity correlation with the help off-axis holography is suggested and discussed. The major goal of the study to measure the complex coherence function of the laser speckle and apply this parameter for imaging through random scattering medium.

3.4.1 Basic principle

The conceptual diagram for the generation of speckles in an observation plane is shown in Figure 3.7. When a quasi-monochromatic coherent source of laser light is incident on a scattering layer, a random spatial distribution of intensity called speckle pattern in the observation plane is generated.

The random distribution of electric field $E_o(r)$ at the observation plane can be written as

$$E_o(r) = \int E_o(\hat{r}) \exp[i\phi(\hat{r})] \exp\left(-\frac{2\pi}{\lambda f} r.\hat{r}\right) d\hat{r} \qquad 3.22$$

where r and $\hat{r}$ are the position vectors in observation/Fourier transform plane and object plane/scattering plane, $E_o(\hat{r})$ is the random field distribution at scattering plane, $\phi(\hat{r})$ corresponds to the random phase distribution arise by scattering plane, λ is the wavelength, f being the focal length of Fourier transforming lens and suffice 'o' for object speckle distribution.

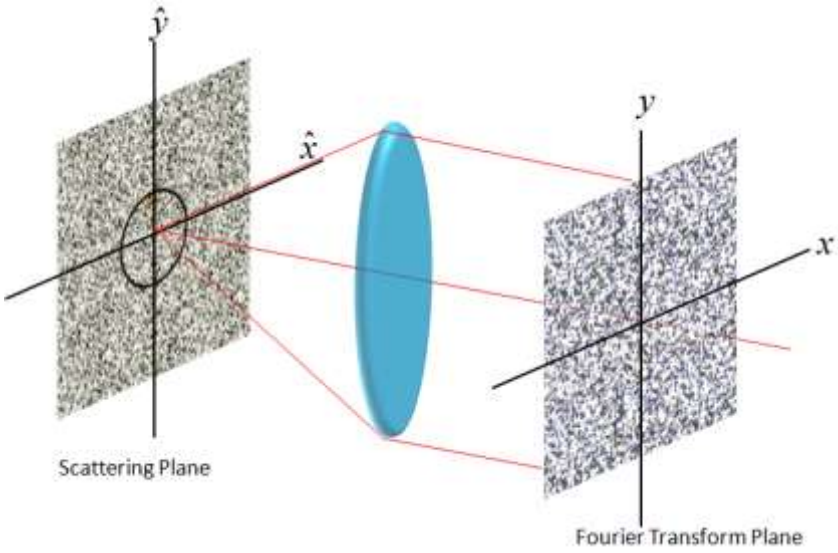

Figure 3.7: Conceptual diagram for speckle generation.

The second order correlation $C_o(r)$ after spatial averaging at the observation plane can be expressed as

$$C_o(\Delta r) = \left\langle E_o^*(r_1) E_o(r_2) \right\rangle_s \quad 3.23$$

$$= \int E_o^*(r_1) E_o(r_1 + \Delta r) dr_1 \quad 3.24$$

Where $\Delta r = r_1 + r_2$, r_1 and r_2 are position vectors in observation plane and $\langle \ \rangle_s$ is spatial average.

For random field obeying Gaussian statistics the relationship between the second order and fourth order correlations can be expressed as

$$K_o(\Delta r) = \left\langle \Delta I_o(r) \Delta I_o(r + \Delta r) \right\rangle_s \quad 3.25$$

The spatial fluctuation of intensity can be written as

$$\Delta I_o(r) = I_o(r) - \left\langle I_o(r) \right\rangle \quad 3.26$$

Where $K_o(\Delta r)$ = covariance function, $\Delta I_o(r)$ = object intensity at Fourier transforming plane, ΔI = spatial fluctuation with respect to mean value of intensity. By using speckle statistics phenomena, the cross covariance function is proportional to modulus square of second order field correlation at same plane, which can be written as

$$K_0(\Delta r) \propto \left| C_o(\Delta r) \right|^2 \quad 3.27$$

As the above equation gives only the amplitude of the complex coherence function, the phase part is lost. The lost phase can be retrieved by employing speckle holographic principle suggested in [18,19]. In this technique, a known independent speckle is added coherently with object speckle to encrypt the phase information of the complex coherence function resulting in speckle hologram. The coherence function for an independent spatially separate reference speckle can be written as

$$W_r(\Delta r) = \int circ\left(\frac{\hat{r} - \hat{r}_g}{a} \right) \exp\left(-i \frac{2\pi}{\lambda f} \Delta r \hat{r} \right) d\hat{r} \quad 3.28$$

where $\hat{r} = \hat{r}_g$ i*mpli*es lateral shift of reference beam of radius 'a' on scattering plane and suffix 'r' stands for reference.

The resultant coherence function at Fourier transforming plane can be expressed as

$$C(\Delta r) = \left\langle E^{*}(r_1) E(r_1 + \Delta r) \right\rangle_s \quad 3.29$$

$$= \left\langle \{E_o(r_1) + E_r(r_1)\}^{*} \{E_o(r_1 + \Delta r) + E_r(r_1 + \Delta r)\} \right\rangle_s \quad 3.30$$

As an assumption that speckles originate from scattering media independent of each other the mutual coherence between the independent and the object coherence function can be neglected.

$$\text{i.e. } \left\langle E_o^{*}(r_1) E_r(r_1 + \Delta r) \right\rangle = 0 \text{ and } \left\langle E_o(r_1 + \Delta r) E_r^{*}(r_1) \right\rangle = 0$$

Therefore, the resultant coherence function takes the form

$$C_H(\Delta r) = C_o(\Delta r) + C_R(\Delta r) \quad 3.31$$

Hence, we get

$$\left| C_H(\Delta r) \right|^2 = \left| C_o(\Delta r) + C_R(\Delta r) \right|^2 \quad 3.32$$

$$= \left| C_0(\Delta r) \right|^2 + \left| C_R(\Delta r)^2 \right| + C_o(\Delta r) C_R^{*}(\Delta r) + C_o^{*}(\Delta r) C_R(\Delta r) \quad 3.33$$

C_o^{*} and C_R^{*} are the complex conjugates of the respective coherence functions

From Equation 3.33, it is clear the complex part of coherence function is encoded in an interferometric equation; with the use of proper techniques, one can recover complex part of correlation function.

3.4.2 Experimental set-up

In this section a pair of experimental set-ups based on the off-axis holography method to retrieve the complex coherence function of the speckle field and the information behind the multiple scattering media is depicted. The first optical set-up is devised for single shot recovery of the object information behind the scattering medium. The second optical set-up is devised to retrieve the flow information behind the scattering medium.

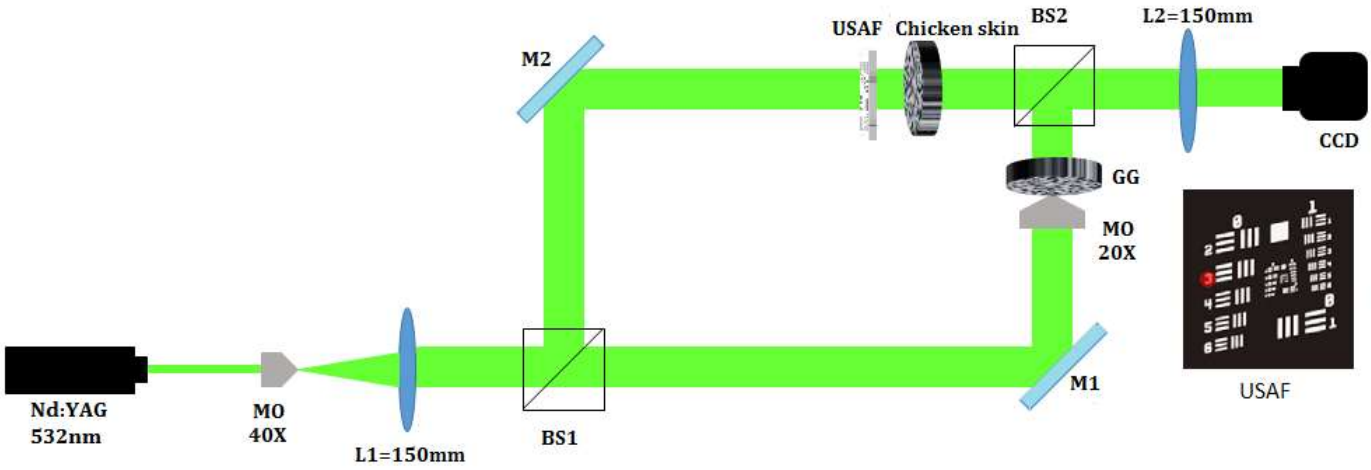

Figure 3.8: Experimental set-up for single shot recovery of object information behind scattering media.

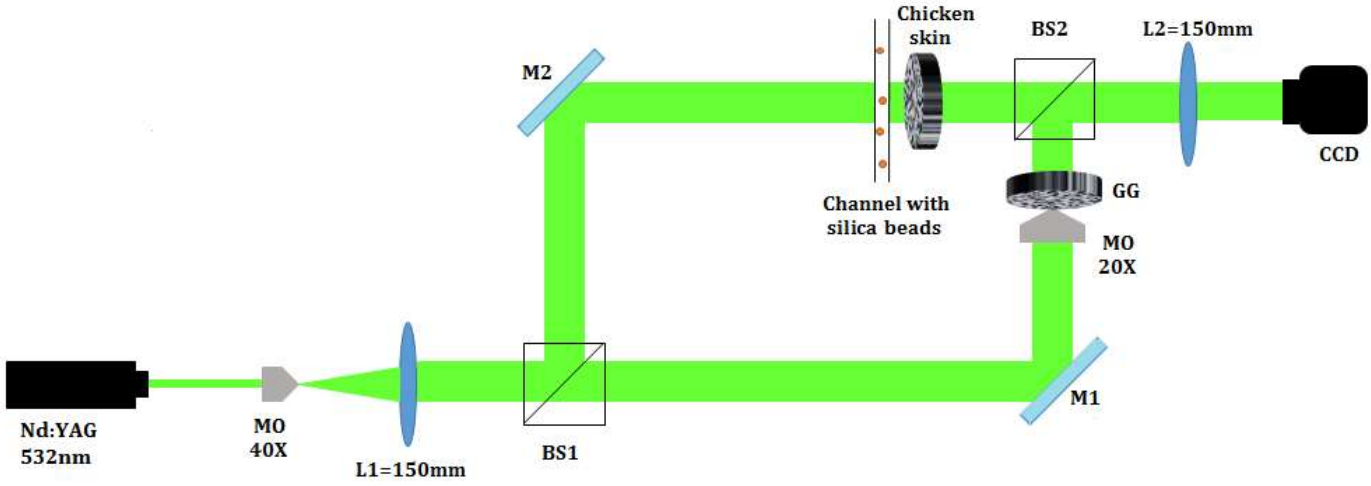

Figure 3.9: Experimental set-up for flow retrieval behind scattering media.

A linearly polarized laser light of wavelength 532nm has been used in the set-ups. The collimated light from the laser source is spatially filtered with the combination of microscopic objective 40X and a pinhole of size 10 micron. The spatially filtered light is collimated with a lens of 150mm and is spatially divided by beam splitter (BS1). The laser beam transmitted through (BS1) act as reference beam while the reflected beam act as the object arm of the interferometer. In the first optical setup the light beam reflected from mirror (M2) is transmitted through object "5" of the USAF chart, while in the second optical setup the light reflected from mirror (M2) is transmitted through small phantom channel in

which the liquid along with the silica beads of diameter of 0.25mm is allowed to flow by using syringe pump. The light beam in the object arm then illuminates the chicken skin and generates the object speckle pattern. The transmitted beam from the beam splitter (BS1) is reflected by mirror (M1) and passes through a microscopic objective 20X and illuminates the ground glass (GG) which generates an independent reference speckle pattern. The object and reference speckle patterns are combined using beam splitter (BS2) and is Fourier transformed using a lens of focal length 150mm. The resultant speckle pattern is captured by the CCD camera, which has a pixel width of 4 micron. The purpose of using Fourier transforming is to maintain spatial stationarity over camera plane.

3.4.3 Recovery of complex coherence function

The resultant speckle hologram formed after the coherent superposition of object and reference speckle is spatially averaged to calculate the covariance function in order to measure complex correlation function. Once the hologram is averaged out fringes will appear, this fringe pattern encodes the phase of correlation function. By employing the Fourier fringe analysis technique on the obtained fringe pattern, we can recover the complex correlation function from the two-point intensity correlation (covariance) function.

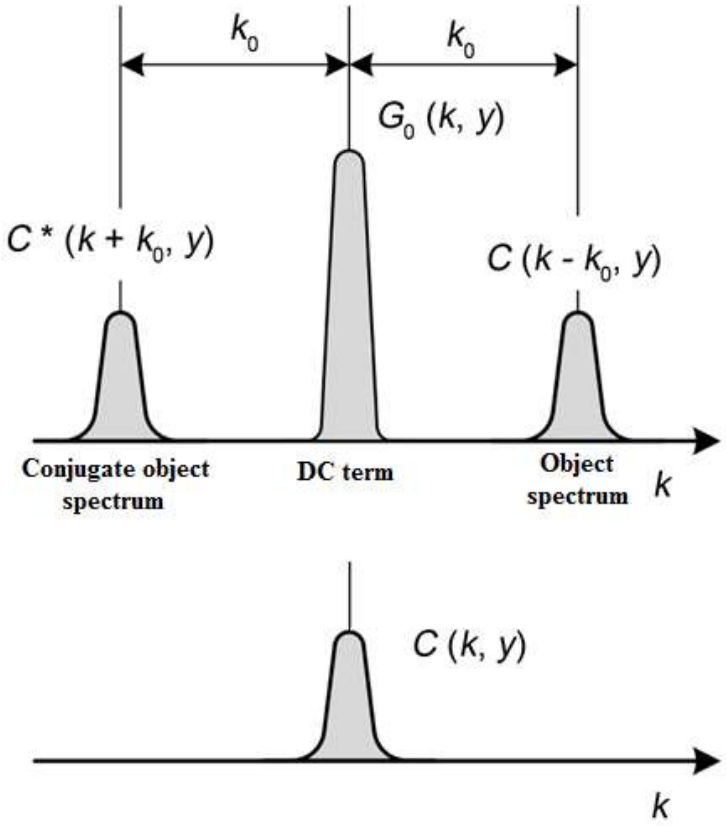

Figure 3.10: Fourier fringe analysis.

By the assumption that complex correlation function of the object speckle is uniform over the object spectrum, we can retrieve the complex mutual coherence function by following the steps as shown in the Figure 3.11.

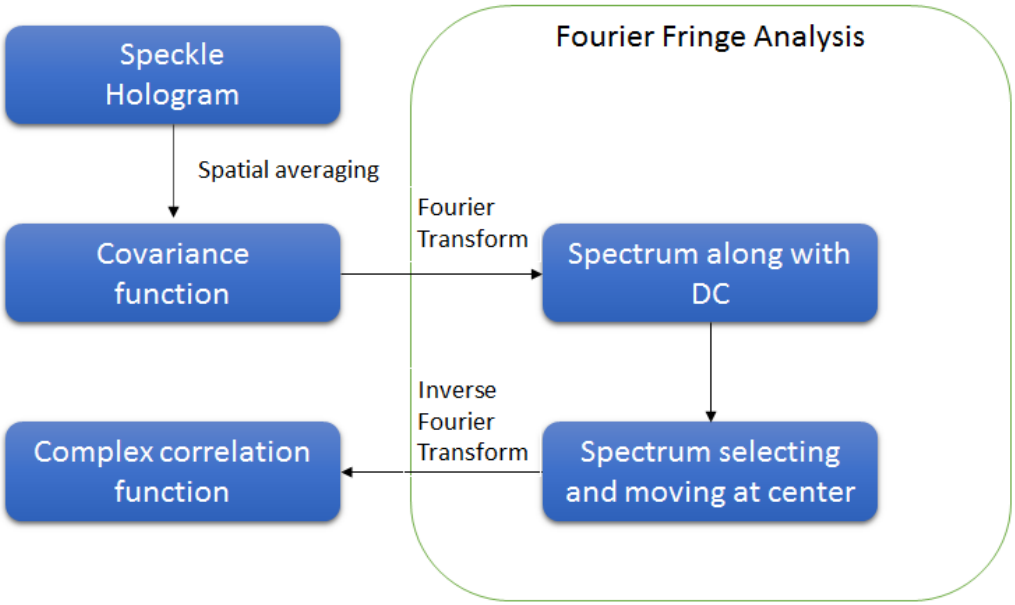

Figure 3.11: Steps involved in retrieving complex correlation function.

3.5 Results and Discussion

The results obtained are represented here in two sections. In first section the results with experimental setup one is demonstrated and in the second section the results with second experimental setup is demonstrated. A detailed discussion and some considerations of the proposed system is also presented.

3.5.1 Section-1 Results with a static test sample

The speckle hologram generated for the object '3' is captured by the CCD and the result is shown in Figure 3.12. The cross covariance of the speckle pattern obtained by spatial averaging is shown in Figure 3.13. Fourier fringe analysis is performed to retrieve the complex correlation function. Figure 3.14 shows the field spectrum along with D.C. The reconstructed object amplitude and phase from the complex correlation function is shown in Figure 3.15 and Figure 3.16.

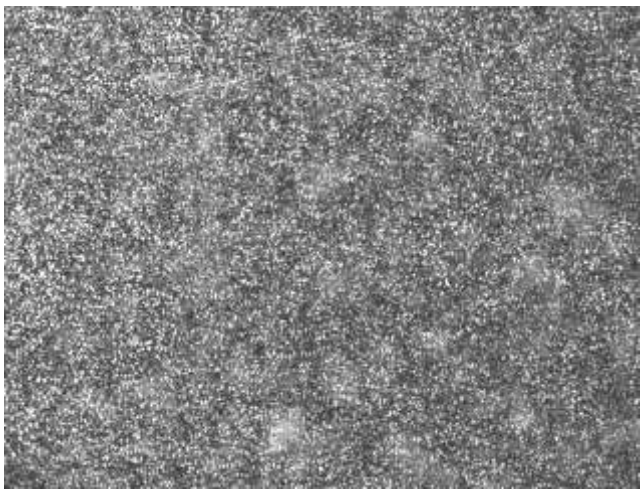

Figure 3.12: laser speckle pattern.

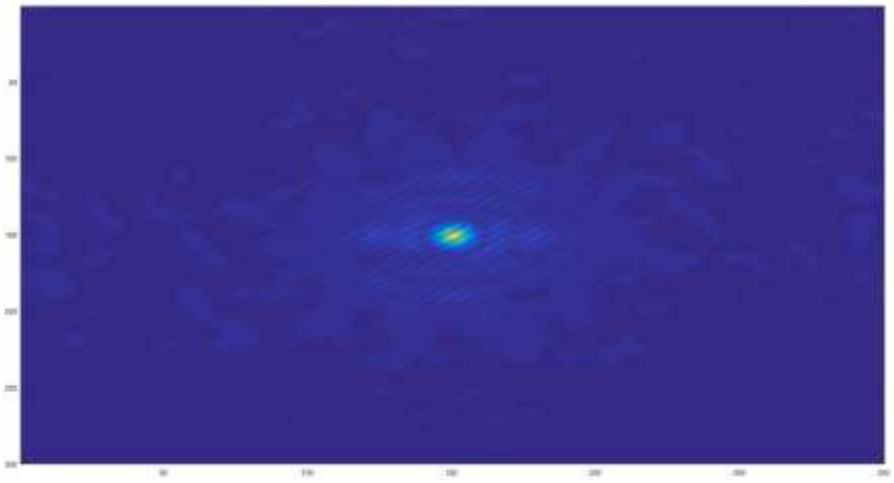

Figure 3.13: Covariance function.

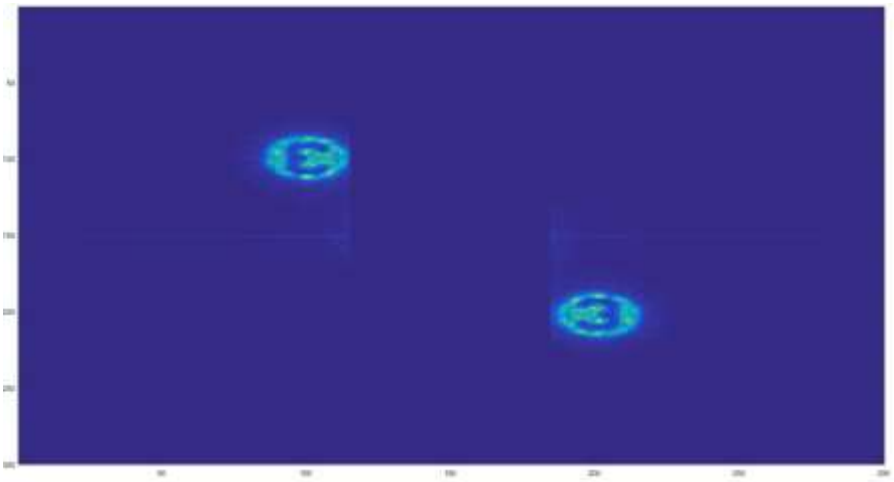

Figure 3.14: Spectrum along with DC.

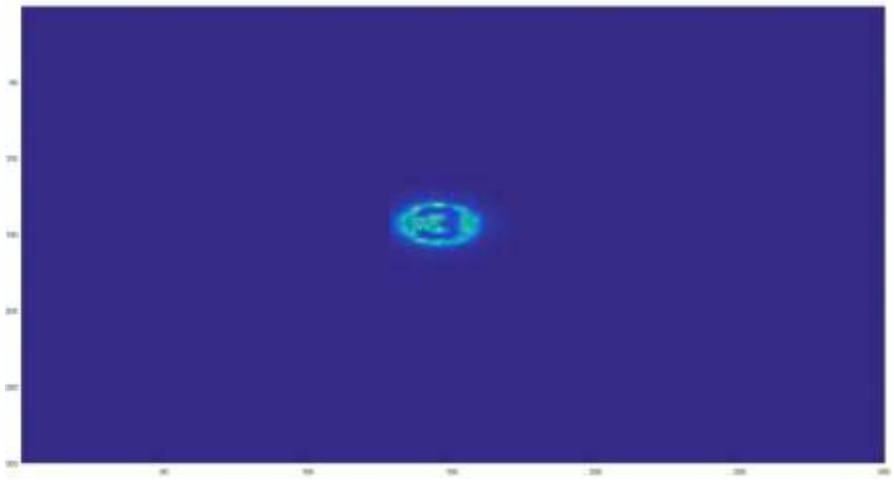

Figure 3.15: Reconstructed object amplitude.

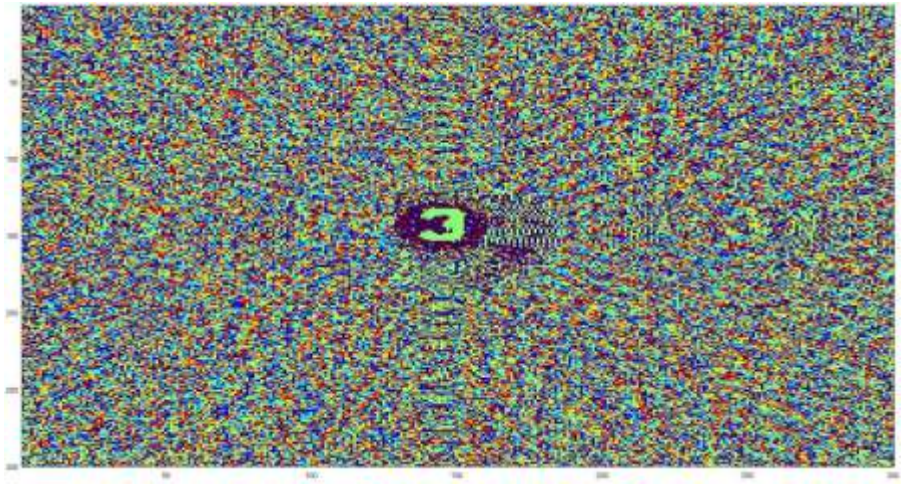

Figure 3.16: Reconstructed object phase.

3.5.2 Section-2 Results with a dynamic test sample

The steps followed for retrieving the flow information behind the scattering media is shown in Figure 3.17. The decomposed speckle frames from the recorded speckle fluctuations is shown in the Figure 3.18. The covariance function of the individual speckle pattern obtained by speckle averaging is shown in Figure 3.19. The reconstructed object amplitude of the decomposed speckle frames is shown in Figure 3.20 (a, b, c). The reconstructed object phase of the decomposed speckle frames is shown in Figure 3.21(a, b, c).

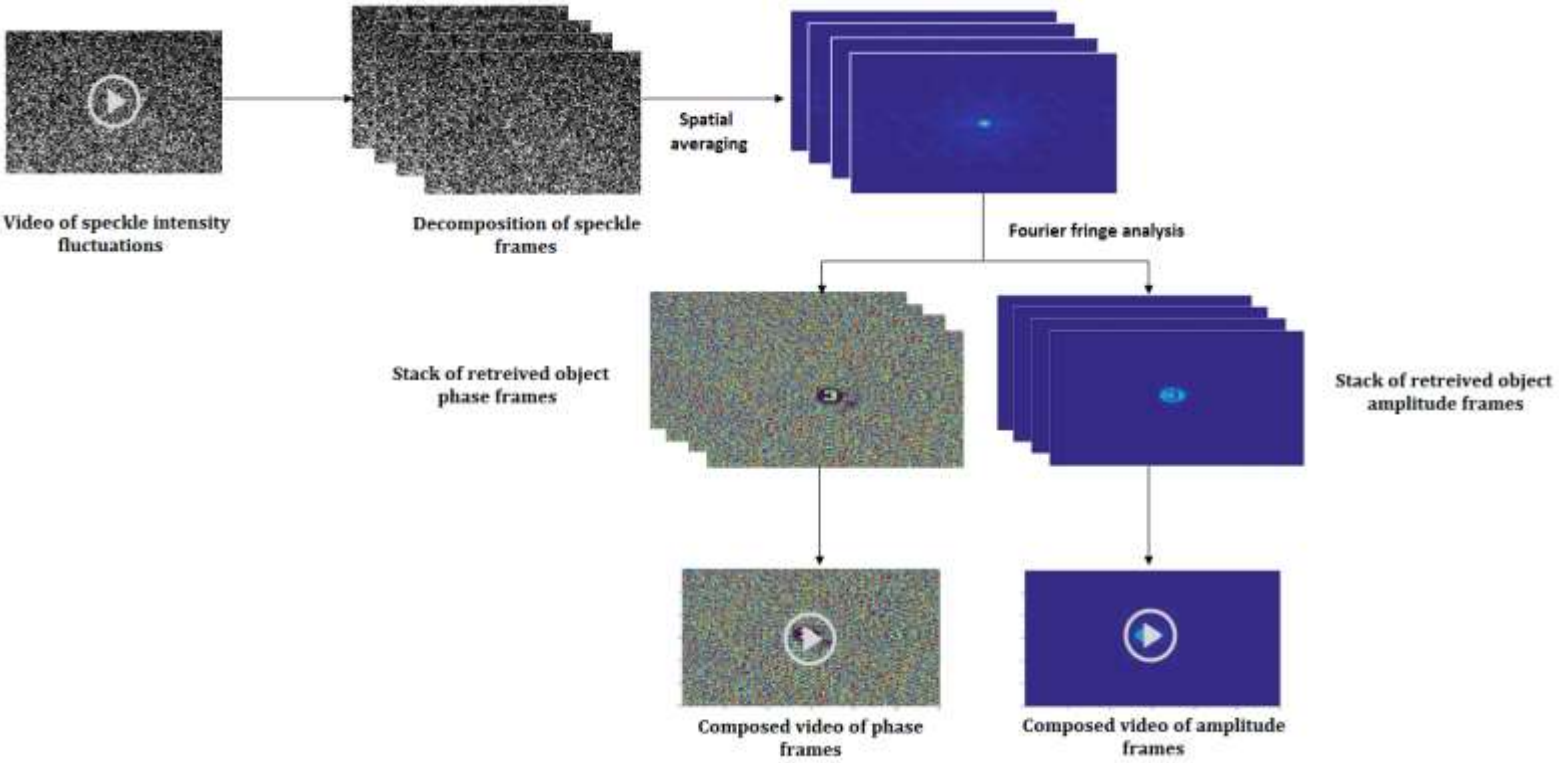

Figure 3.17: Steps involved in retrieval of flow behind the scattering media.

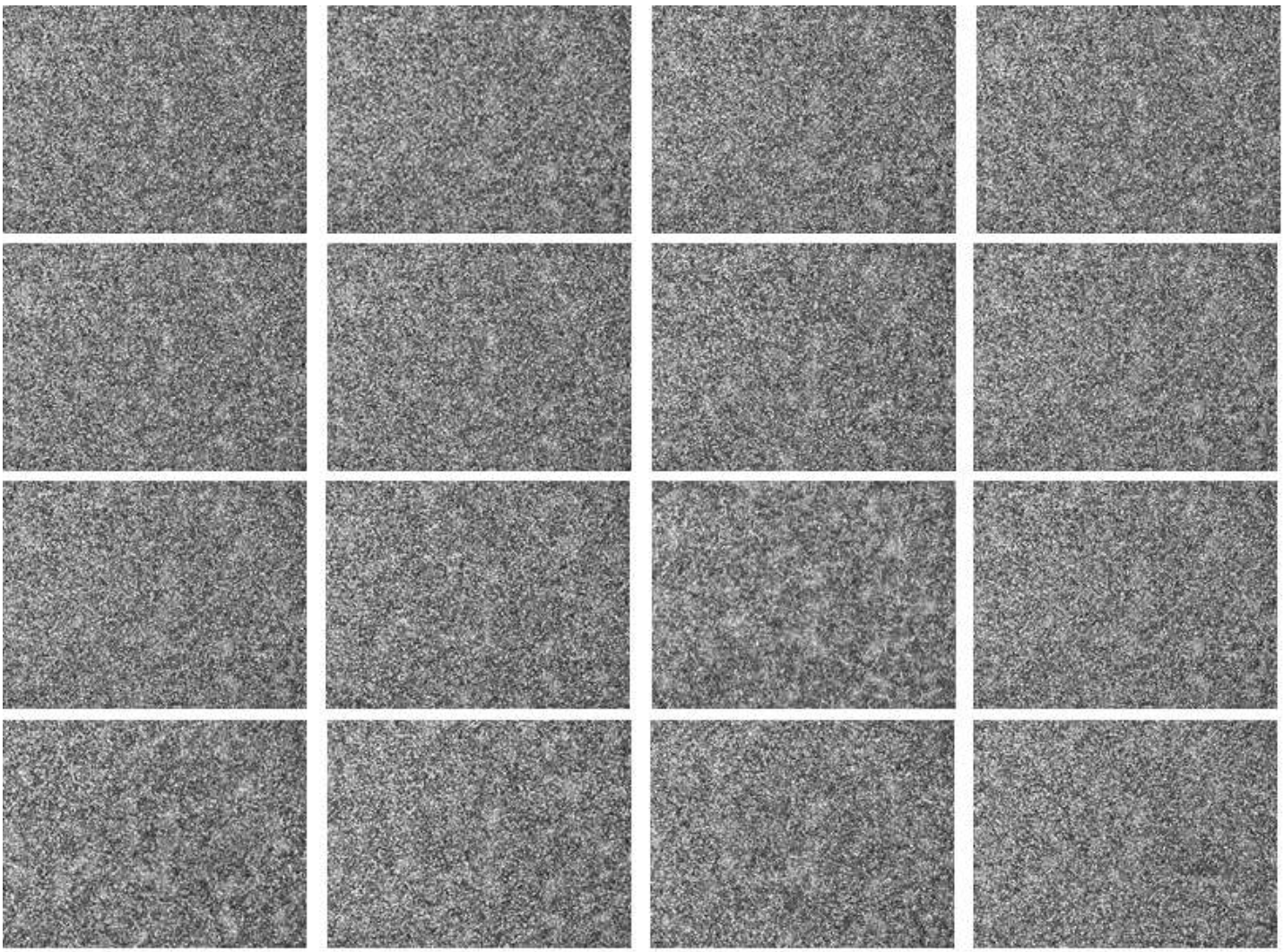

Figure 3.18: Decomposed speckle frames from the recorded video (In order left to right).

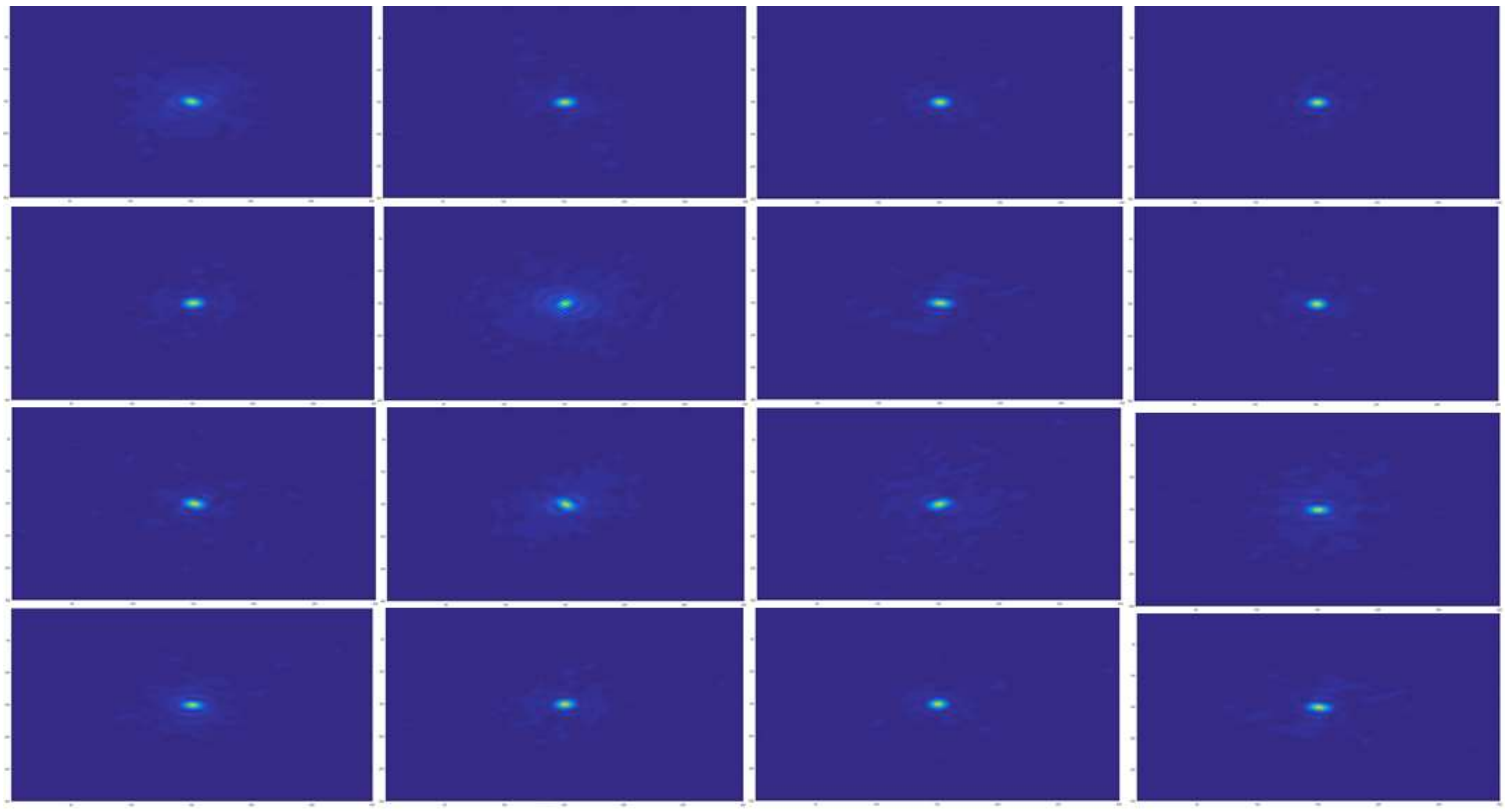

Figure 3.19: Covariance function of the decomposed speckle frames (In order left to right).

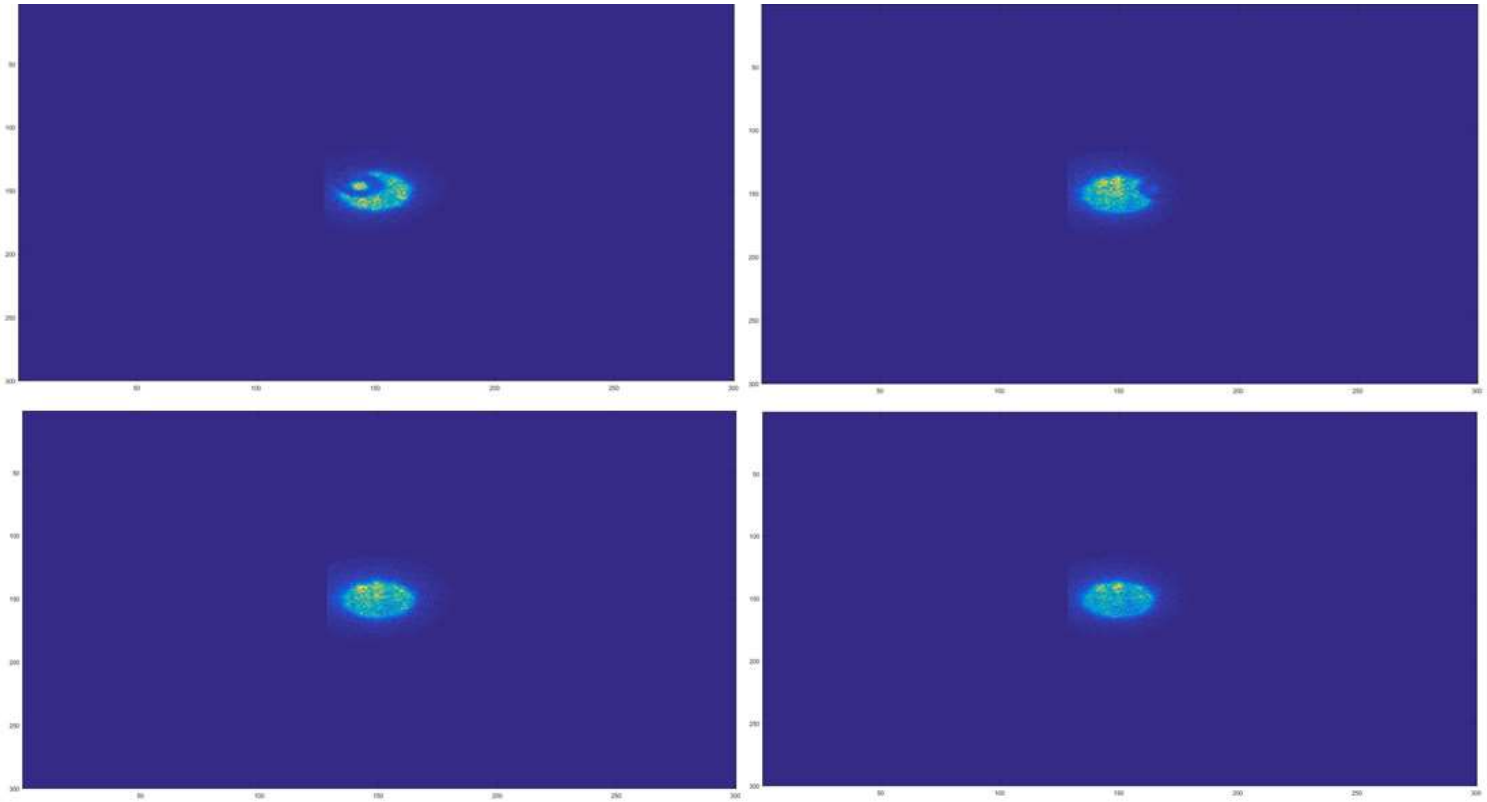

Figure 3.20 (a).

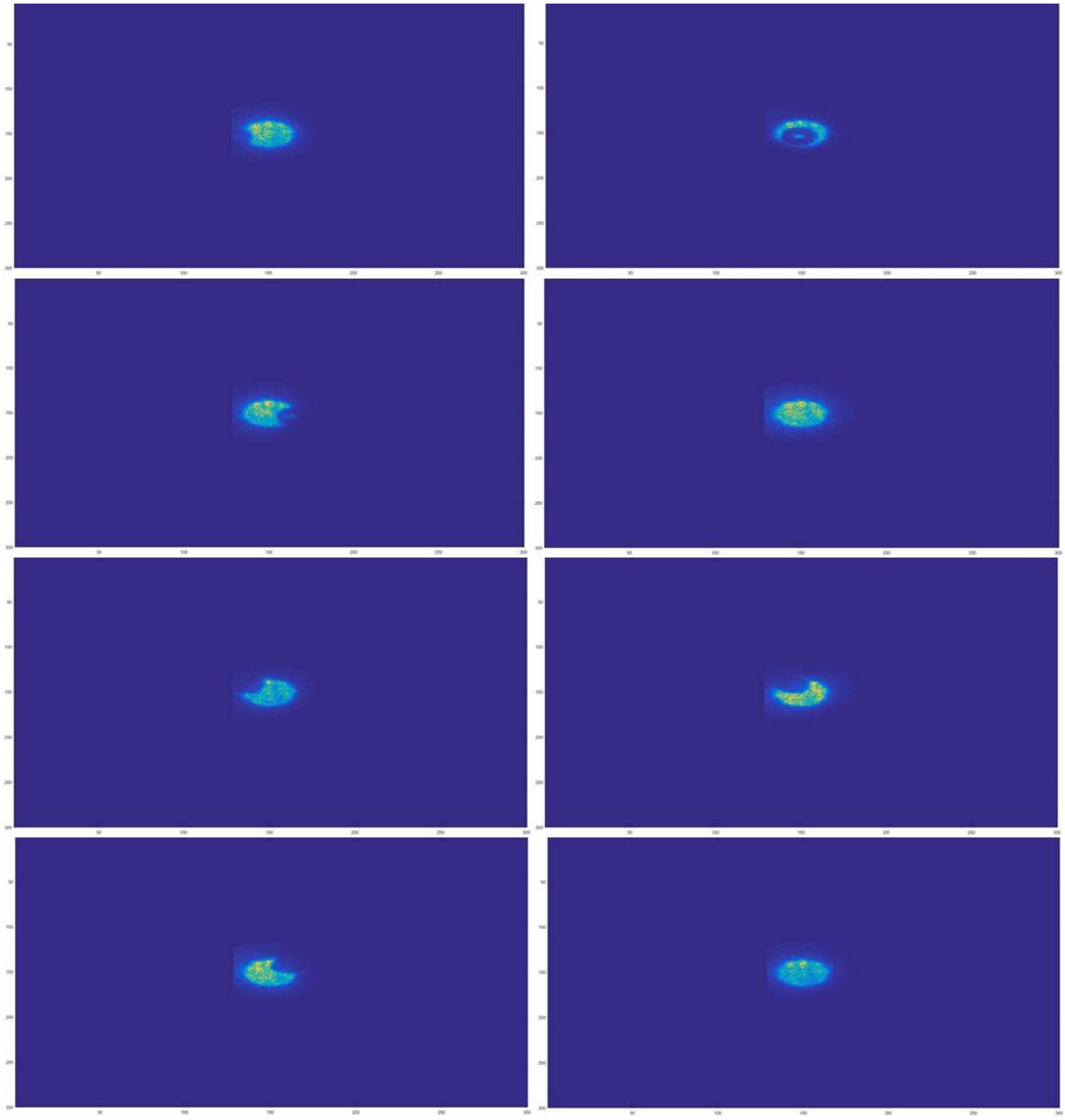

Figure 3.20 (b).

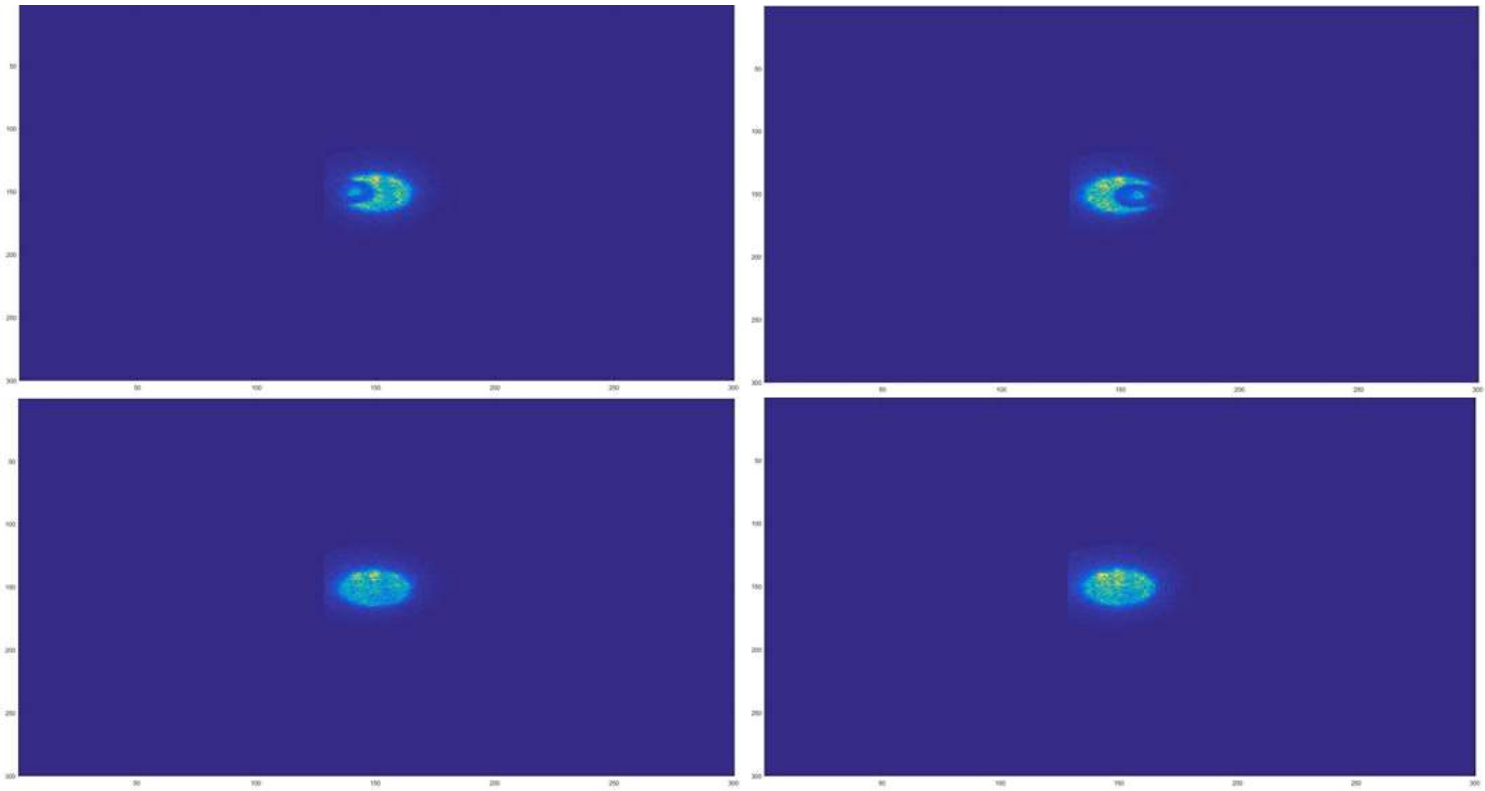

Figure 3.20 (c).

Figure 3.20 (a-c): Reconstructed amplitude information of flow behind scattering media (In order left to right).

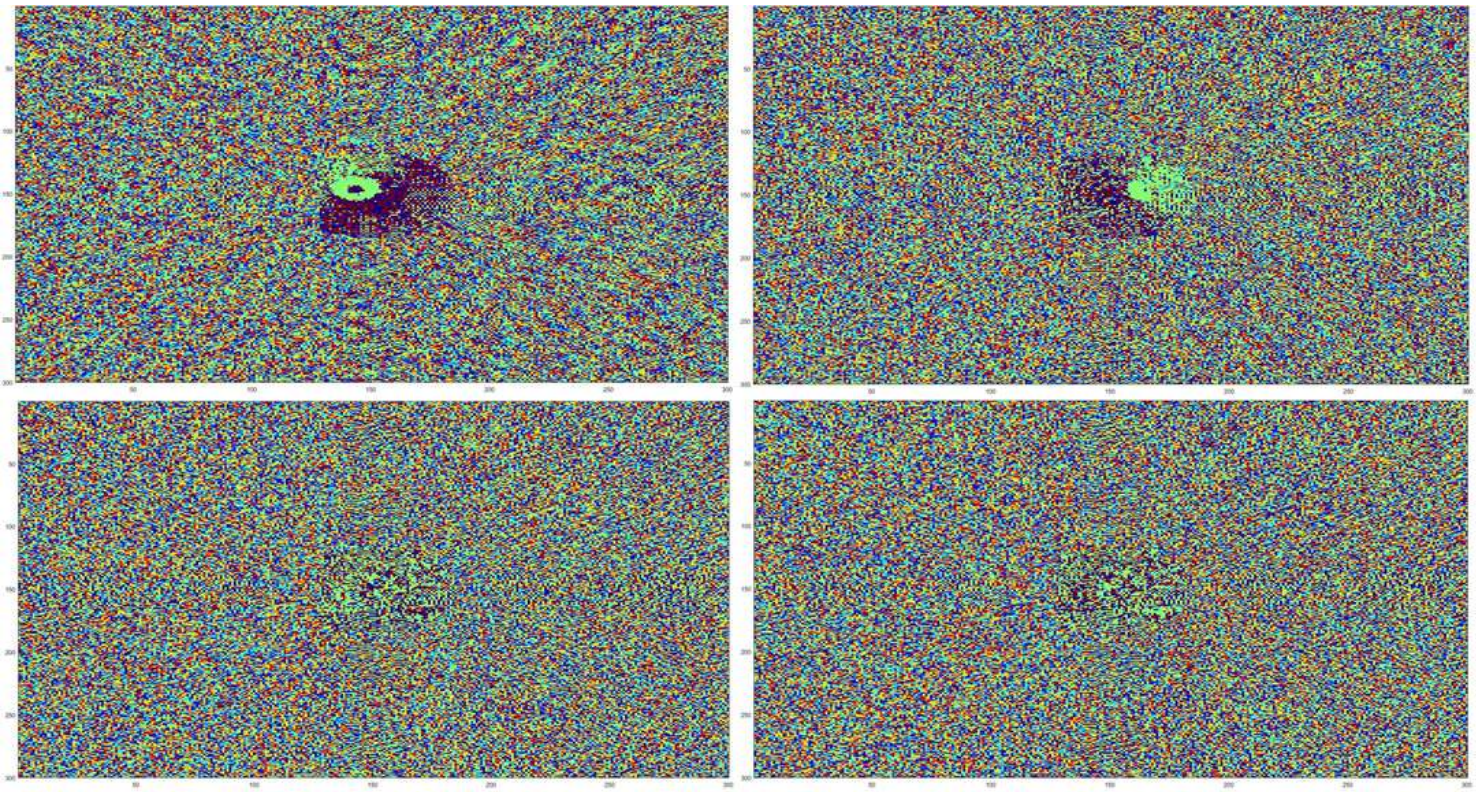

Figure 3.21 (a).

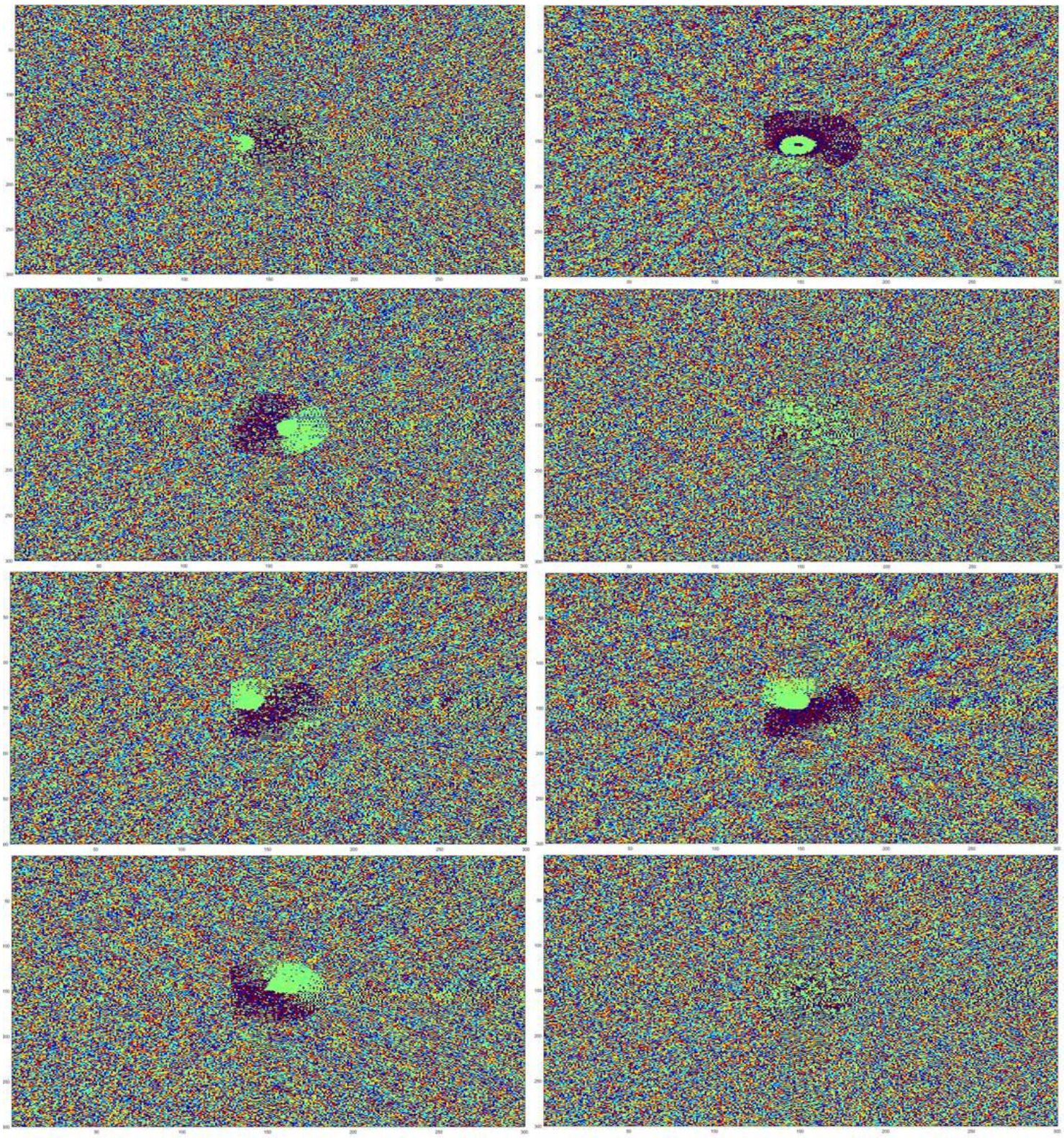

Figure 3.21 (b).

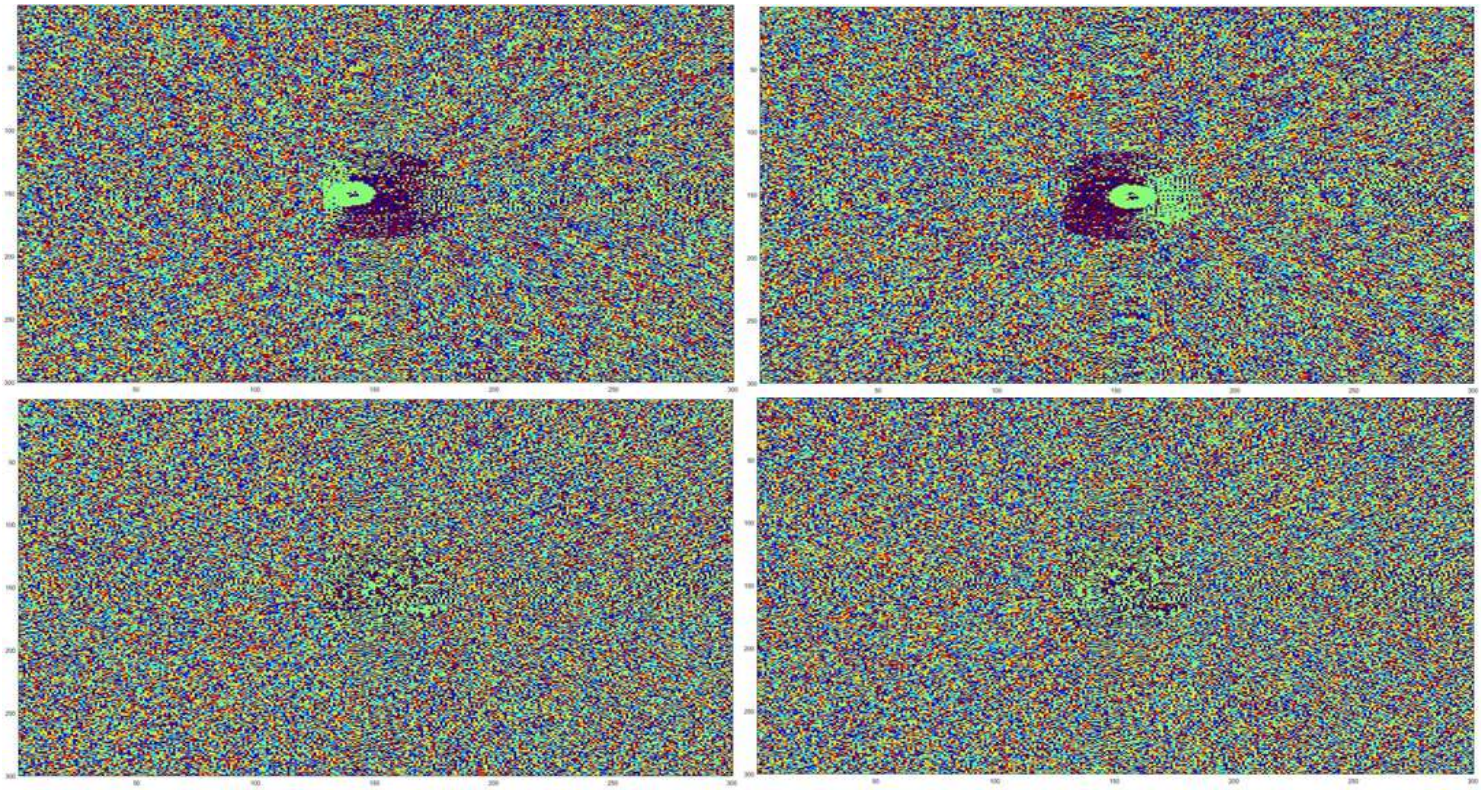

Figure 3.21 (c)

Figure 3.21(a-c): Reconstructed phase information of flow behind scattering media (In order left to right).

Chapter 4

Multi Contrast Microscopy with Sequential LED Array Illumination

4.1 Introduction

Optical microscopy is a ubiquitous tool in diverse disciplines, providing detailed visualization of materials and biological specimens [20]. Continuous advancements in the microscopy over the past decades have introduced many new imaging modalities. However bright field, dark field and phase contrast microscopy still represents the most common and widely employed label free imaging methods. Bright field (BF) microscopy provides images by mapping the intensity modulation of the light passing through a specimen. Although it is a simple and most common form of microscopy, it is not suitable for observing translucent samples such as unlabeled cells and thin tissues as they do not exhibit strong attenuation in visible light [21]. Dark field microscopy produces high contrast images of thin samples being sensitive to the edges of the specimen by employing oblique light illumination beyond the maximum illumination angle that the optical system can capture, thereby minimizing the un-scattered background while collecting the scattered light from the sample [22]. Phase contrast microscopes such as Zernike [23,24] and Differential interference contrast [25.26] microscopy provides images by rendering optical phase delay of light passing through a specimen in to intensity distribution. These methods operate on the principle of light and thus require specialized optical components to form an interferometer in the imaging setup. Although bright field, dark field and phase contrast images offer complementary information of specimens, simultaneous acquisition of images is not feasible in conventional microscopes, since each modality requires a distinct optical arrangement and dedicated optical elements such as annular condensers and specialized objective lenses to form an interferometer in the imaging setup. The scope of this work is to develop a microscope capable of tri-modal imaging by employing programmable LED array as an illumination unit in microscopy.

4.2 Multi contrast imaging with sequential LED array illumination

Appropriate illumination of the specimen is necessary to obtain high quality images in microscopy [27]. Conventional microscopes are equipped with Kohler illumination setup which was first introduced in 1893 by August Kohler for specimen illumination. Recently more advanced illumination schemes have also been reported in in recent years including Structured illumination, light sheet illumination [28, 29], focus grid illumination [30] and non-diffracted Bessel beam illumination [31]. With the maturation in LED technology, the use of LED array as the light source can provide several cost and usage advantages over Kohler illumination source. The replacement of the optical condenser with programmable LED array paves the way for tri-modal imaging by sequential illumination of the LED's.

To understand the proposed system let us consider only one LED lit in the LED array. The location of the LED can be denoted as (x_i, y_i) as shown in the figure 4.1. Assuming the distance in the Z direction between the LED array and specimen is H, the illumination NA of this LED can be defined as

$$NA = \frac{r}{\sqrt{r^2 + H^2}} \tag{4.1}$$

Where $r = \sqrt{(x_i - x_c)^2 + (y_i - y_c)^2}$, (x_c, y_c) is the location of LED matrix center.

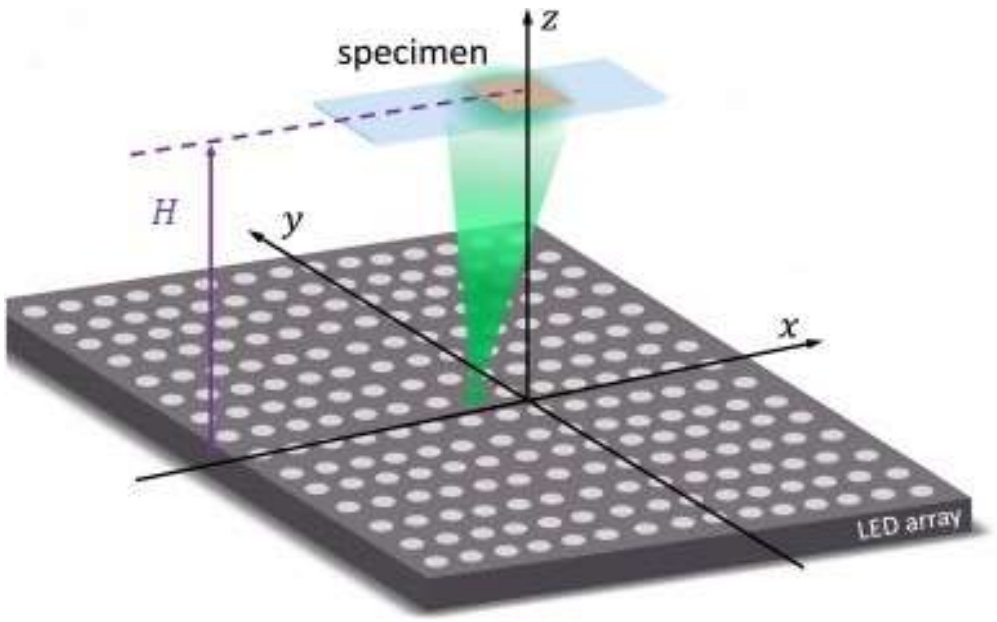

Figure 4.1: LED array source.

4.2.1 Bright field

In the conventional microscopic systems, the bright field image is acquired by matching illumination numerical aperture (NA) to the collection numerical aperture (NA). In the proposed scheme, the numerical aperture for each LED is calculated by using Equation 4.1. In order to achieve the bright field illumination the group of LED's whose illumination NA is greater than that of the collection NA is made to lit [27]. The illumination scheme and the light path for bright field image acquisition is shown in the Figure 4.3.

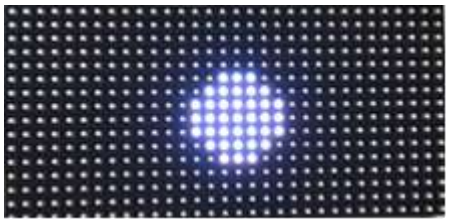

Figure 4.2: Bright field illumination pattern.

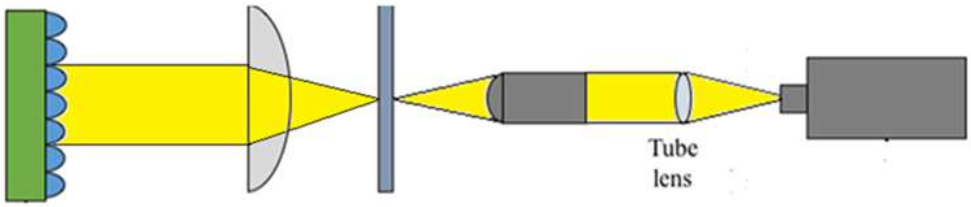

Figure 4.3: light path for bright field image acquisition.

4.2.2 Dark field

For dark field illumination the group of LED is whose illumination numerical aperture is less than that of the collection numerical aperture is made to lit [27]. The illumination scheme and the light path for dark field image acquisition is shown in the Figure 4.4 and Figure 4.5.

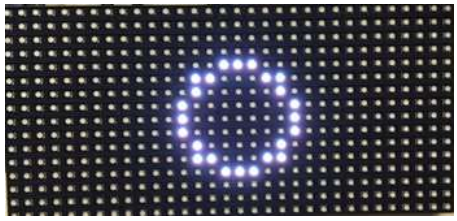

Figure 4.4: Dark field illumination pattern.

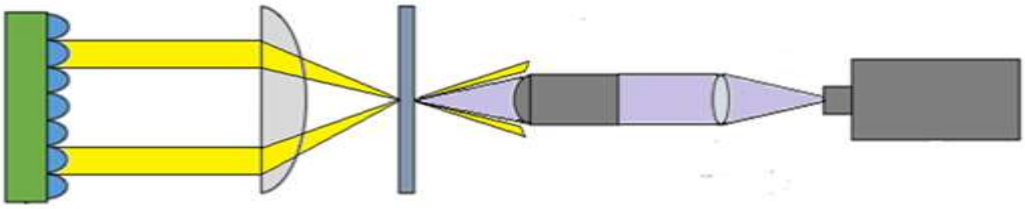

Figure 4.5: Light path for dark field image acquisition.

4.2.3 Phase contrast

Phase contrast imaging works under the principle differential phase contrast (DPC) in which the gradient phase can be extracted from a pair of intensity images taken with opposite illumination angles [32]. To achieve DPC the sample is illuminated by using different asymmetric half circle source patterns i.e. either with left half circle and right half circle or top half circle and bottom half circle as shown in the Figure 4.6. The DPC images is then computed as the normalized difference between the images using

$$I_{DPCLR} = \frac{I_L - I_R}{I_L + I_R}$$
$$I_{DPCTB} = \frac{I_T - I_B}{I_T + I_B} \qquad 4.2$$

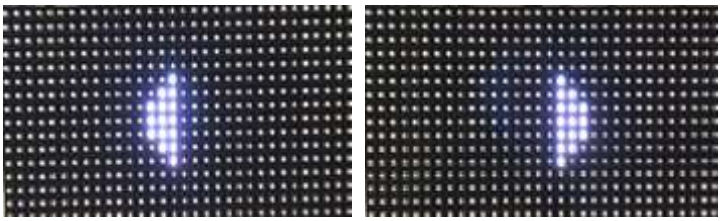

(a) (b)

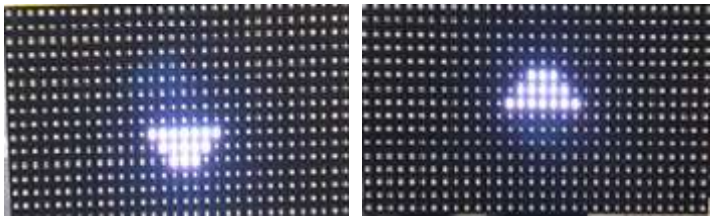

(c) (d)

Figure 4.6 (a-d): Differential Phase contrast illumination patterns.

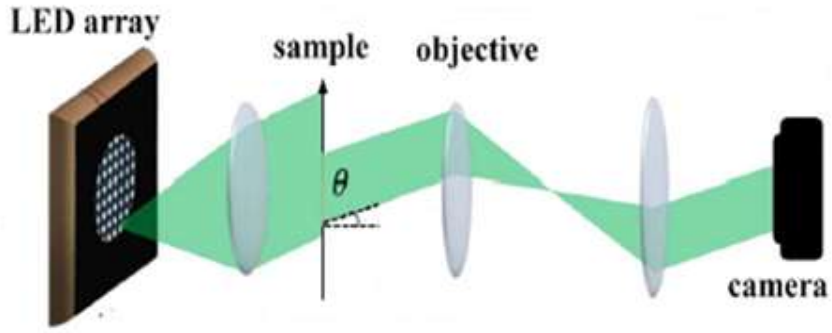

Figure 4.7: Light path for asymmetric illumination.

4.3 Experimental set-up

The experimental set-up for multi contrast microscopy employs a conventional microscopic platform with commercially available Adafruit 16 by 32 LED array matrix controlled by an Arduino microcontroller unit as a source. The light from the LED array source is focused to illuminate the specimen using a Carl Zeiss condenser lens of 0.55 NA. The diffracted light from the specimen is then collected by using a 40X objective lens and is focused on to the image plane by using a tube lens of focal length 165mm. The resultant image at the image plane is captured by using CCD camera of pixel width 6.7 micron.

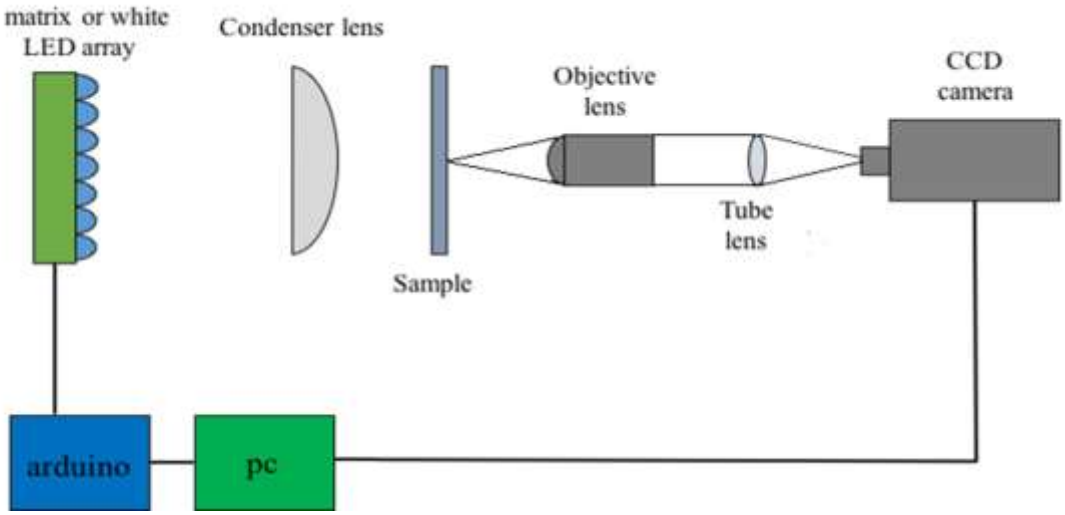

Figure 4.8: Experimental set-up for multi-contrast microscopy.

4.4 Quantitative phase reconstruction

The quantitative phase interpretation of the differential phase contrast (DPC) images proceeds as follows. The local wave front tilt induced by the sample in x and y directions can be calculated from the differential phase contrast (DPC) images using the equation.

$$\begin{bmatrix} \theta_x \\ \theta_y \end{bmatrix} = -NA \begin{bmatrix} I_{DPCLR} \\ I_{DPCTB} \end{bmatrix} \tag{4.3}$$

Where NA is the numerical aperture.

The relation between the wave front tilt and phase gradient is given by

$$\vec{\nabla}\phi(x,y) = \frac{2\pi}{\lambda}\vec{\theta}(x,y) \tag{4.4}$$

Where λ is the mean illumination wavelength, ϕ is the local phase shift in radians induced by the samples.

The complex phase gradient $G(x,y)$ is given by

$$G(x,y) = \nabla_x \phi(x,y) + i\nabla_y \phi(x,y) \tag{4.5}$$

As the measurement of $\vec{\nabla}\phi$ is quantitative, we can integrate to obtain the quantitative estimate of ϕ. This is performed by the complex Fourier integration [33, 34] as given by the equation. The quantitative phase estimate $\phi(x,y)$ is given by

$$\phi(x,y) = \mathrm{Im}\left[F^{-1}\left[\begin{matrix} \dfrac{F\{G(x,y)\times FOV\}}{2\pi(k_x + ik_y)} & |k| \neq 0 \\ C & |k| = 0 \end{matrix} \right] \right] \tag{4.6}$$

Where F corresponds to discrete Fourier transform, C is an arbitrary integration constant, FOV is the image field of view expressed in same physical units as that of λ and k_x, k_y corresponds to Fourier spatial frequencies.

4.5 Results

The experiment is carried out for different phase objects and the results for the bright field, dark field and phase contrast imaging schemes are demonstrated along with the retrieved quantitative phase estimation.

4.5.1 Microfluidic channel

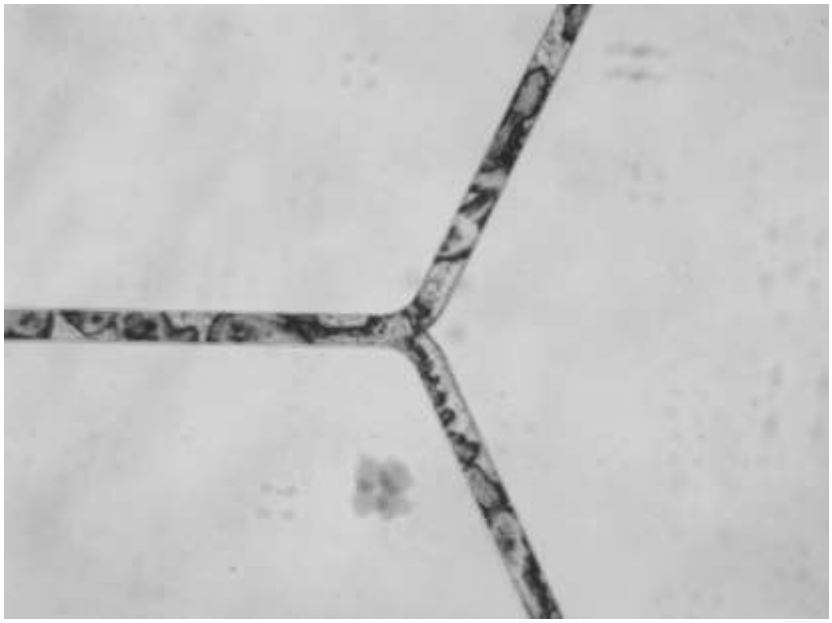

Figure 4.9: Bright field image of microfluidic channel.

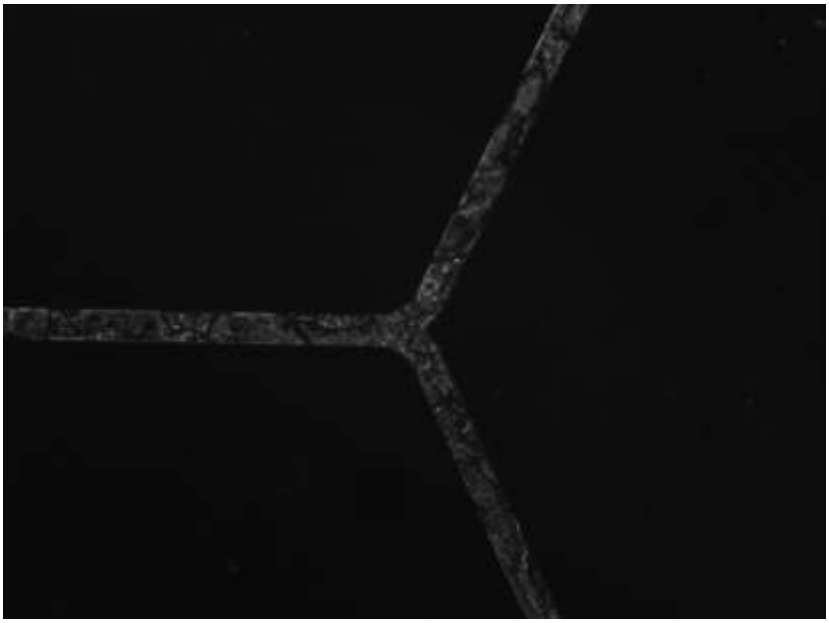

Figure 4.10: Dark field image of microfluidic channel.

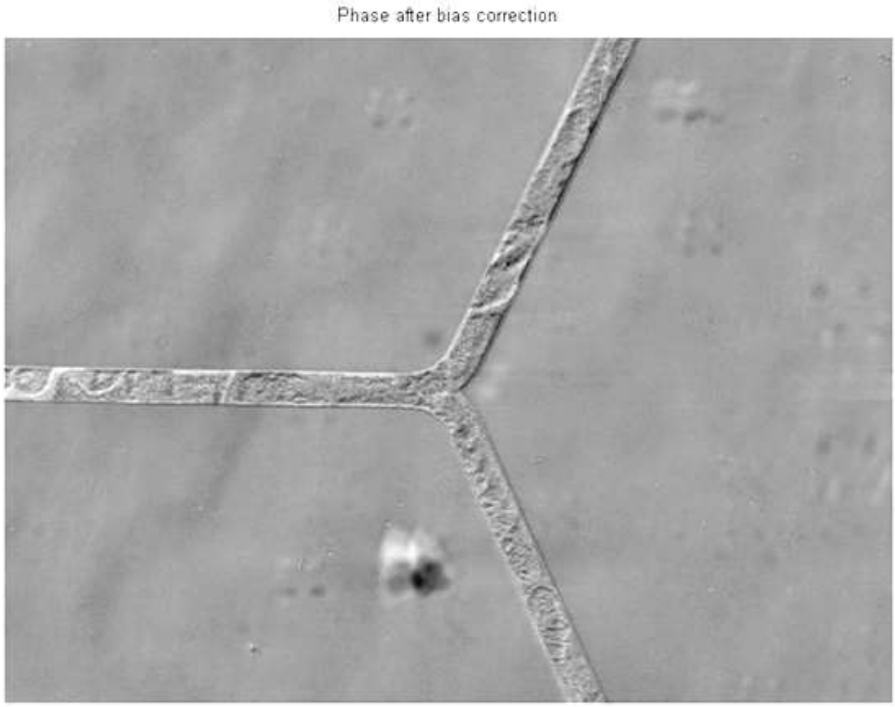

Figure 4.11: Phase contrast image of microfluidic channel.

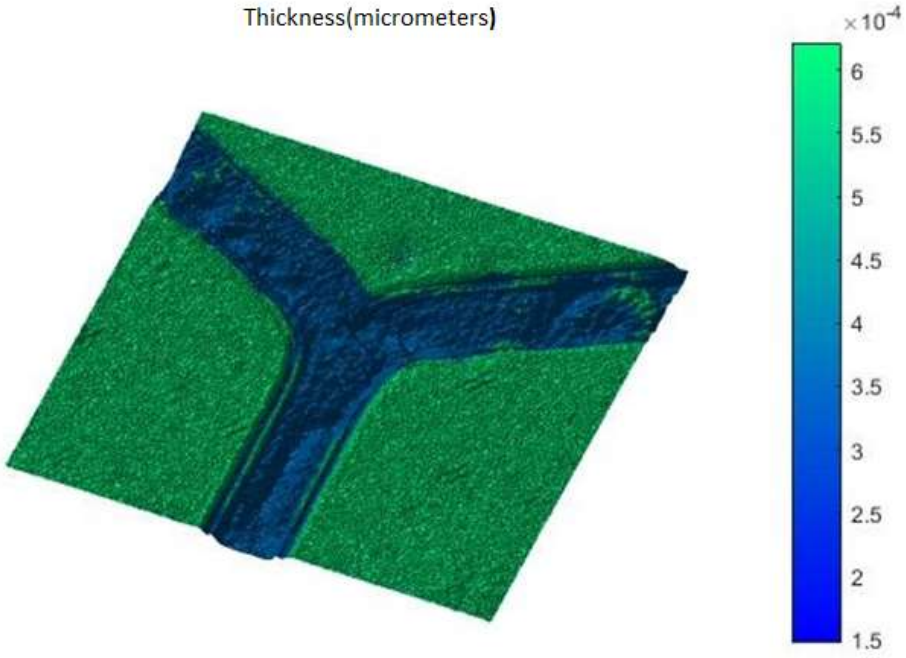

Figure 4.12: Retrieved quantitative phase estimate of microfluidic channel.

4.5.2 Micro beads

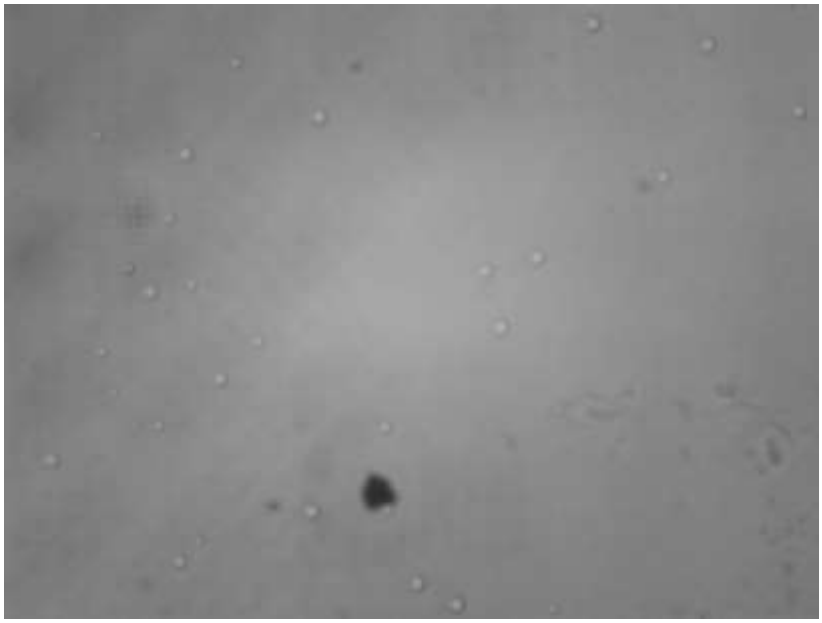

Figure 4.13: Bright field image of microbeads.

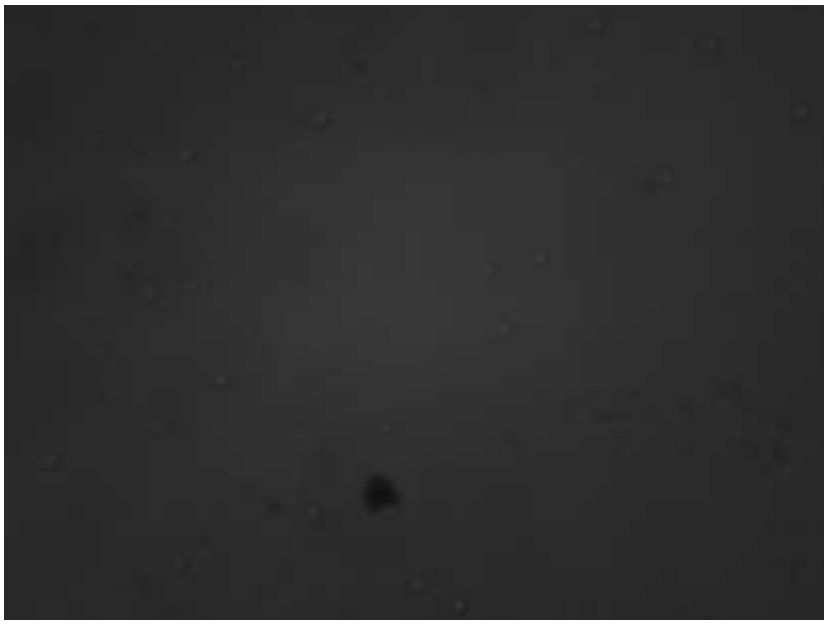

Figure 4.14: Dark field image of microbeads.

Figure 4.15: Phase contrast image of microbeads.

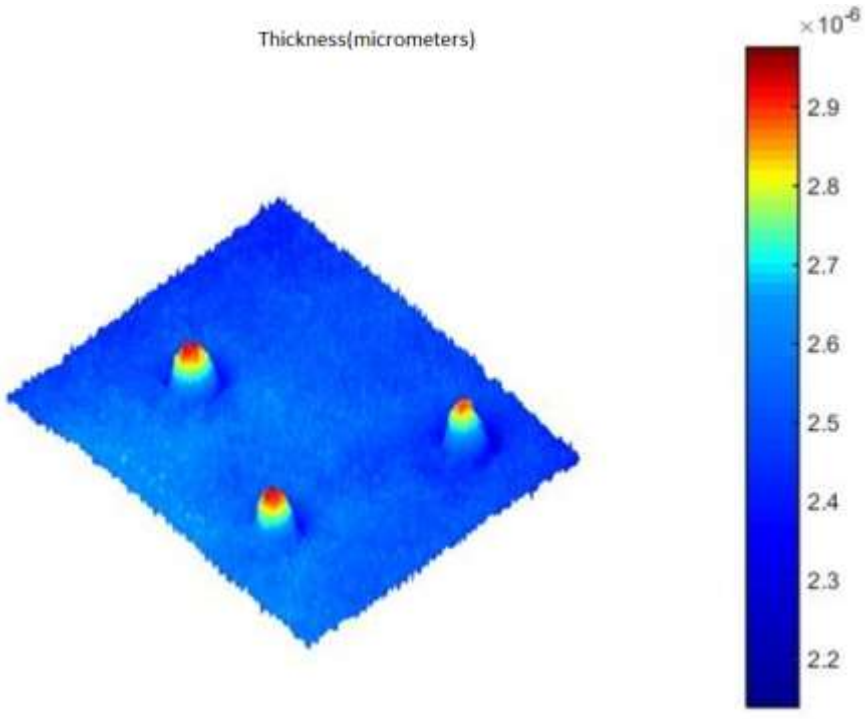

Figure 4.16: Retrieved quantitative phase estimate of microfluidic channel.

4.5.3 Plant cell

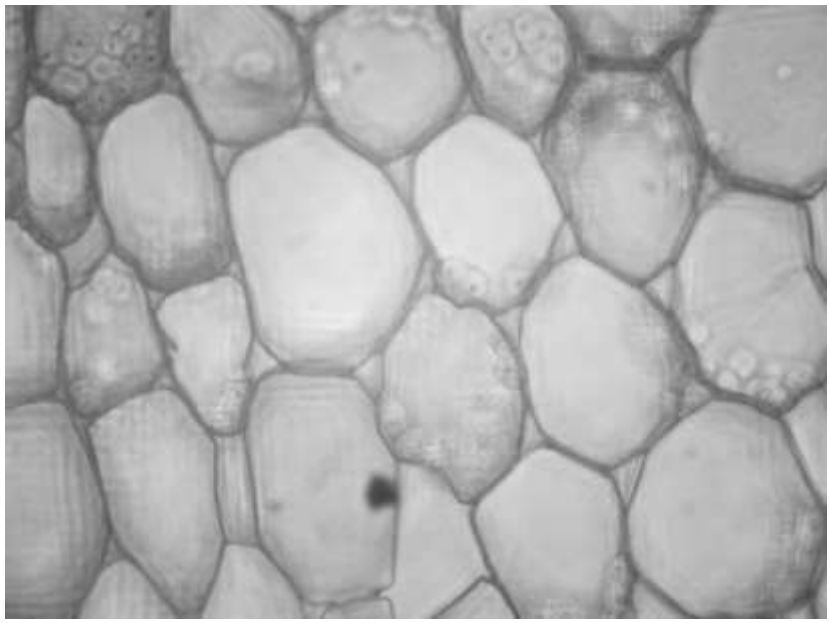

Figure 4.17: Bright field image of plant cell.

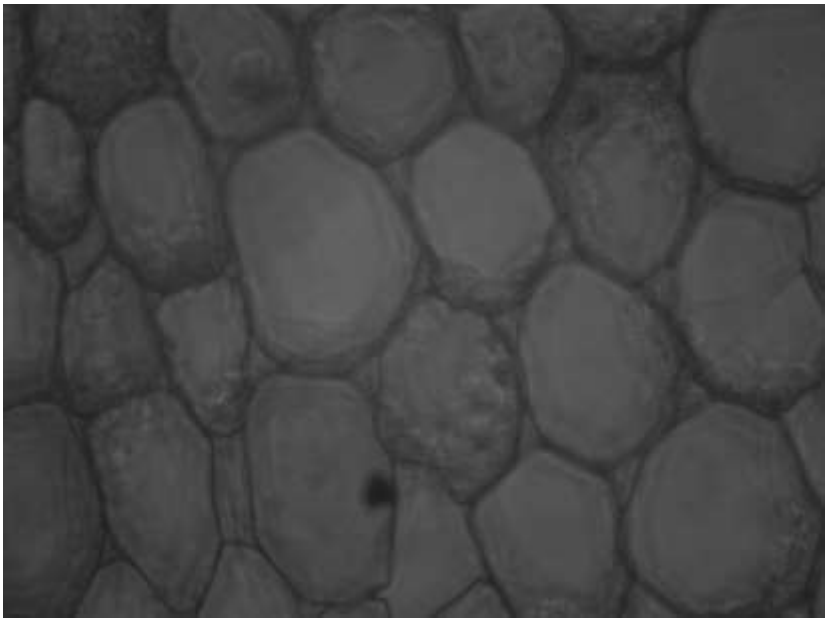

Figure 4.18: Dark field image of plant cell.

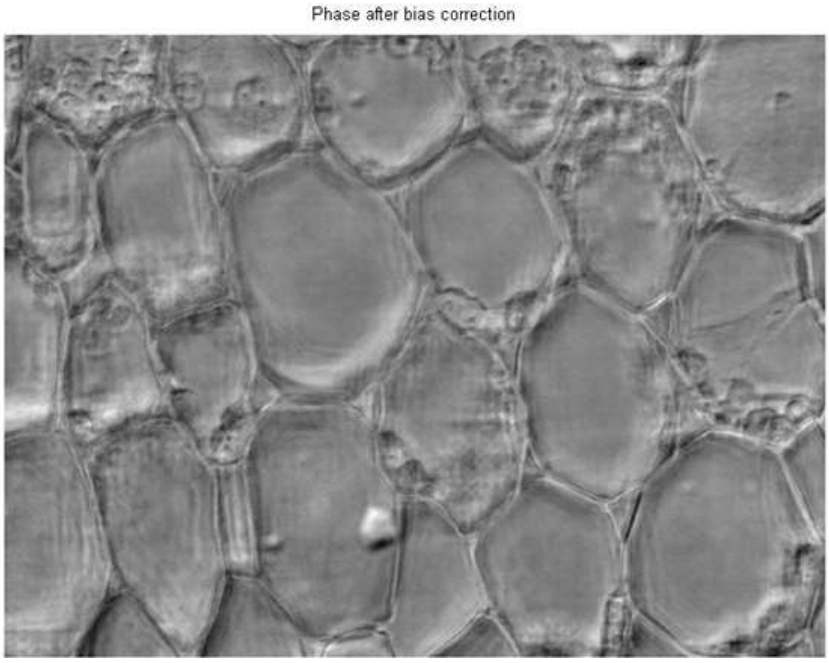

Figure 4.19: Phase contrast image of microbeads.

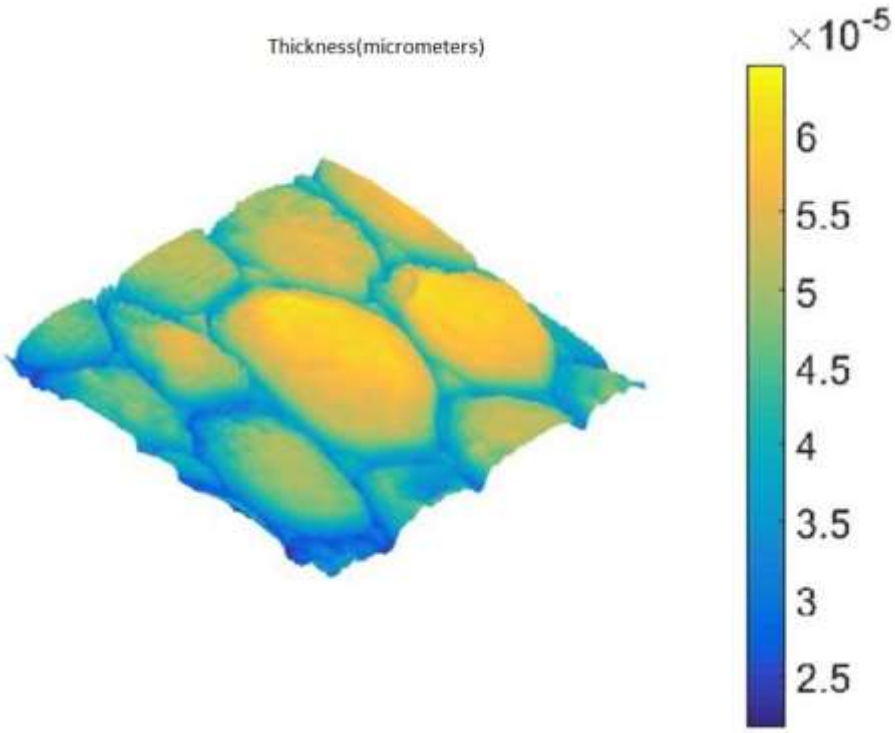

Figure 4.20: Retrieved quantitative phase estimate of plant cell.

4.5.4 Red blood cell

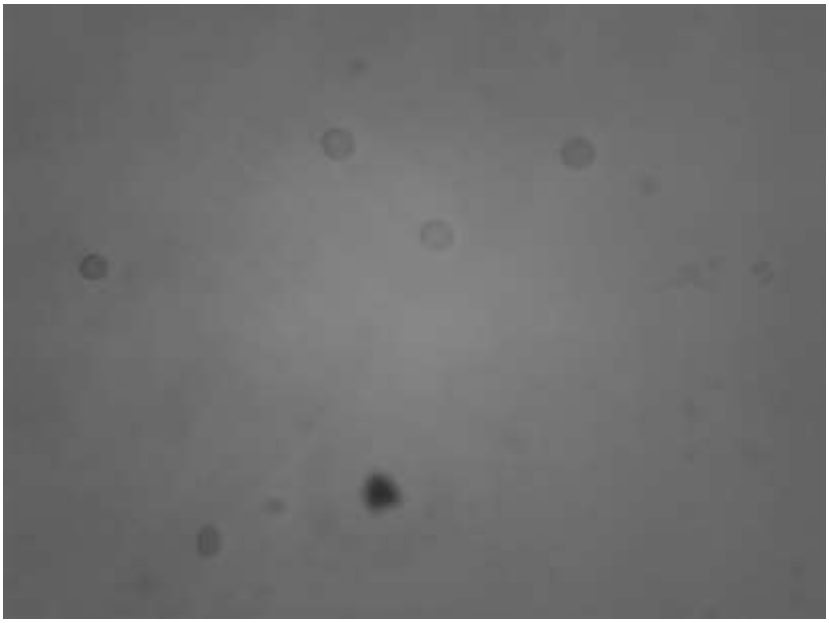

Figure 4.21: Bright field image of red blood cell.

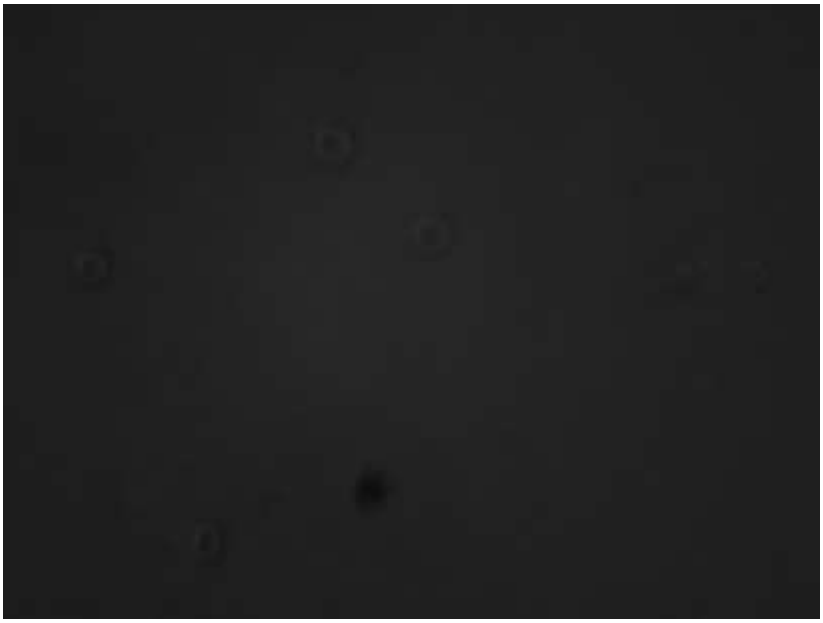

Figure 4.22: Dark field image of red blood cell.

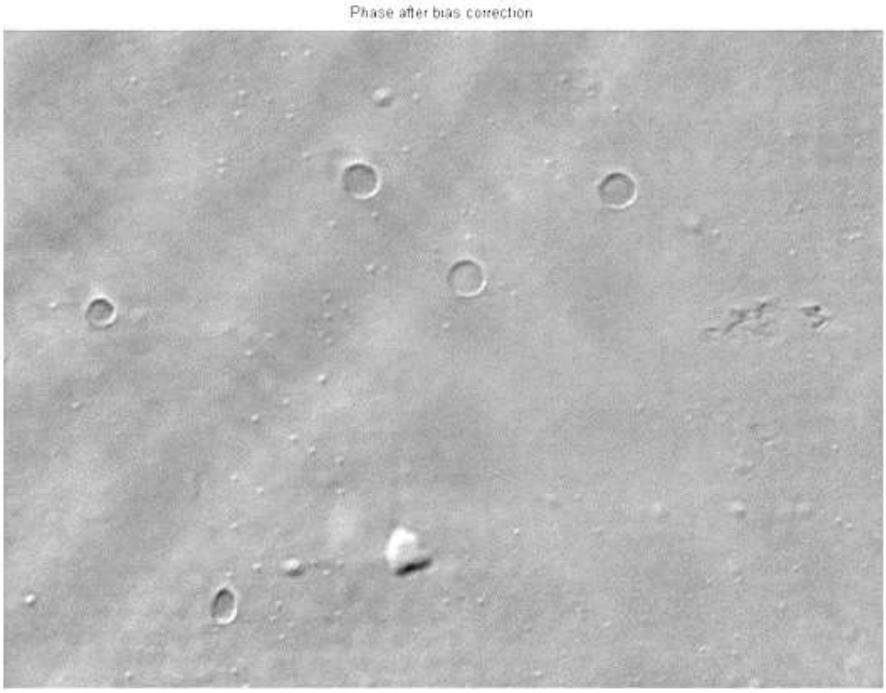

Figure 4.23: Phase contrast image of red blood cell.

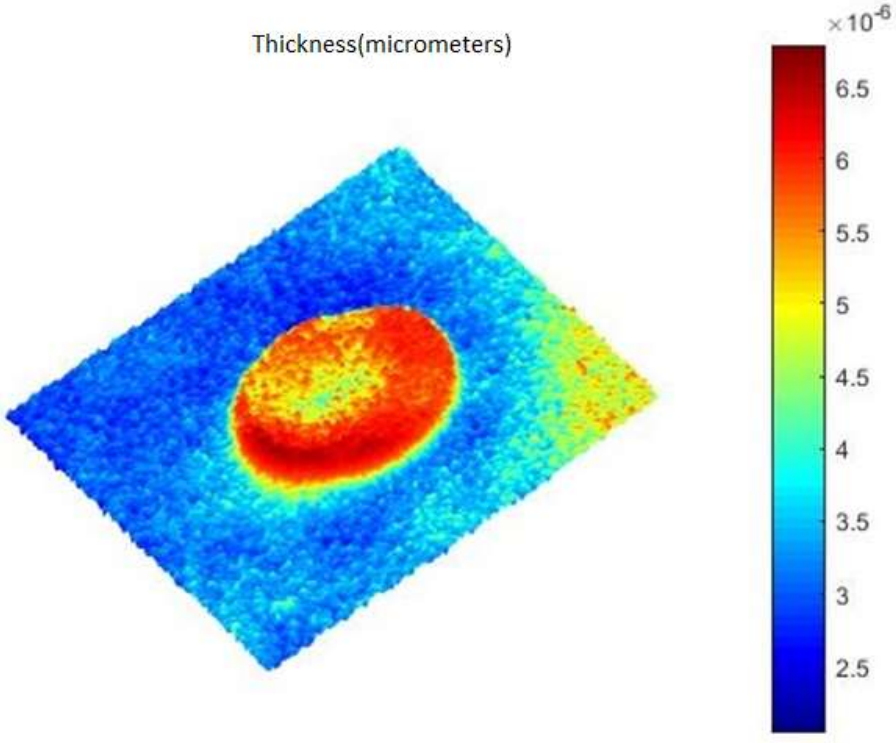

Figure 4.24: Retrieved quantitative phase estimate of red blood cell.

4.5.5 Yeast cell

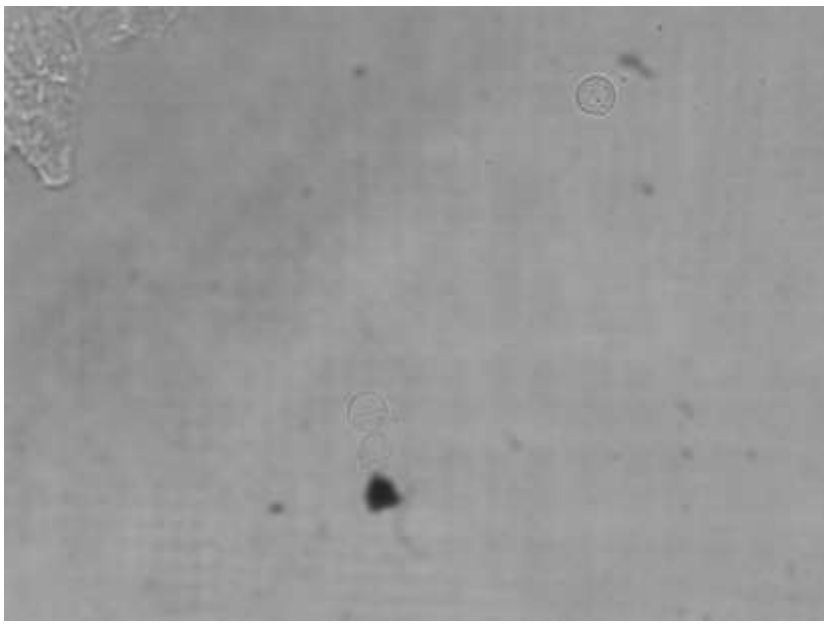

Figure 4.25: Bright field image of yeast cell.

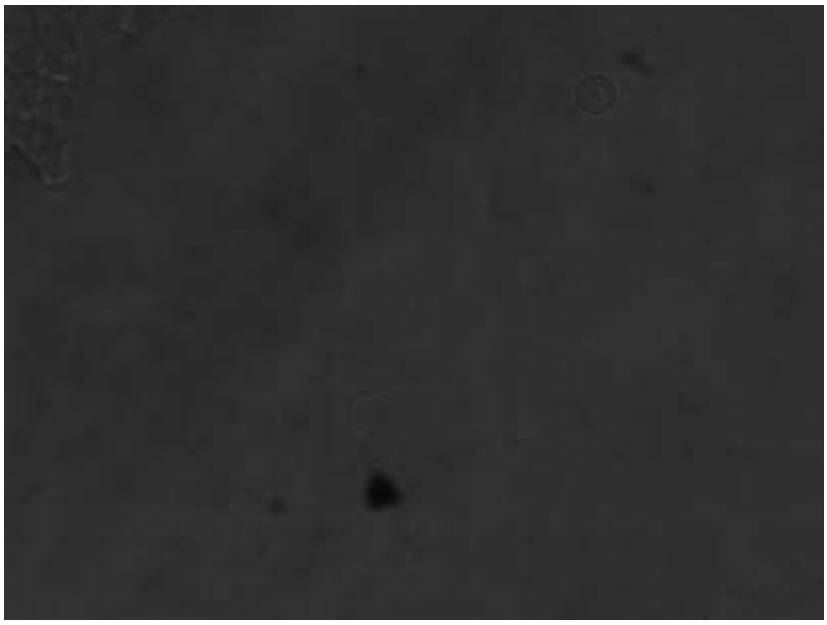

Figure 4.26: Dark field image of yeast cell.

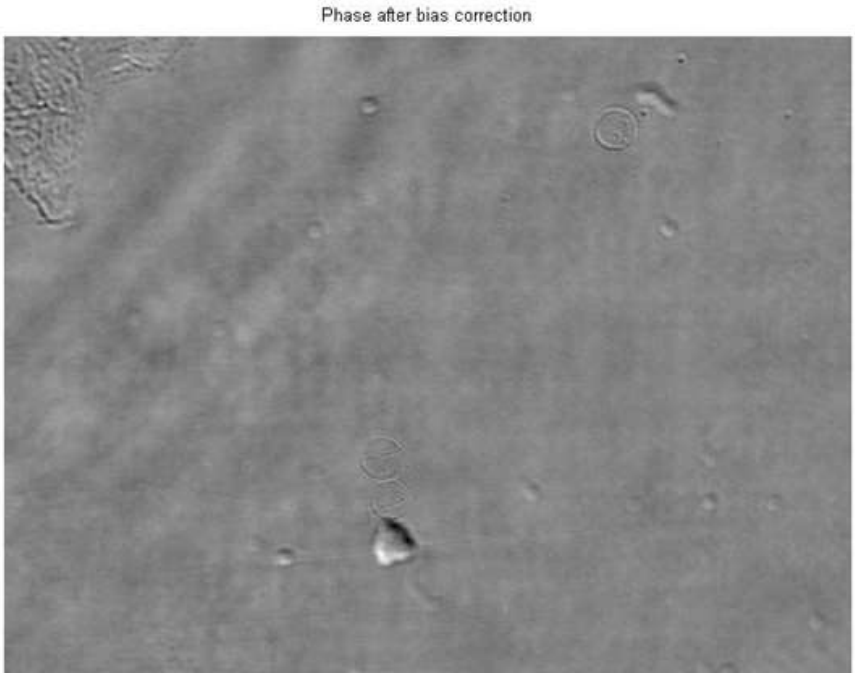

Figure 4.27: Phase contrast image of red blood cell.

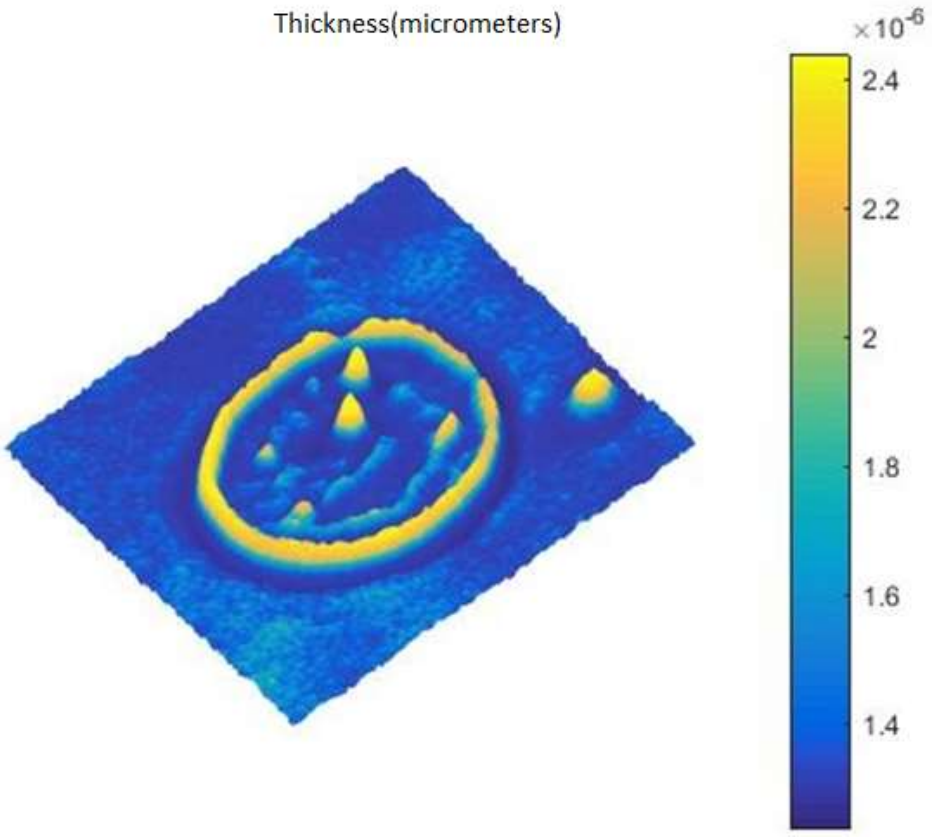

Figure 4.28: Retrieved quantitative phase estimate of red blood cell.

4.5.6 Frog blood cell

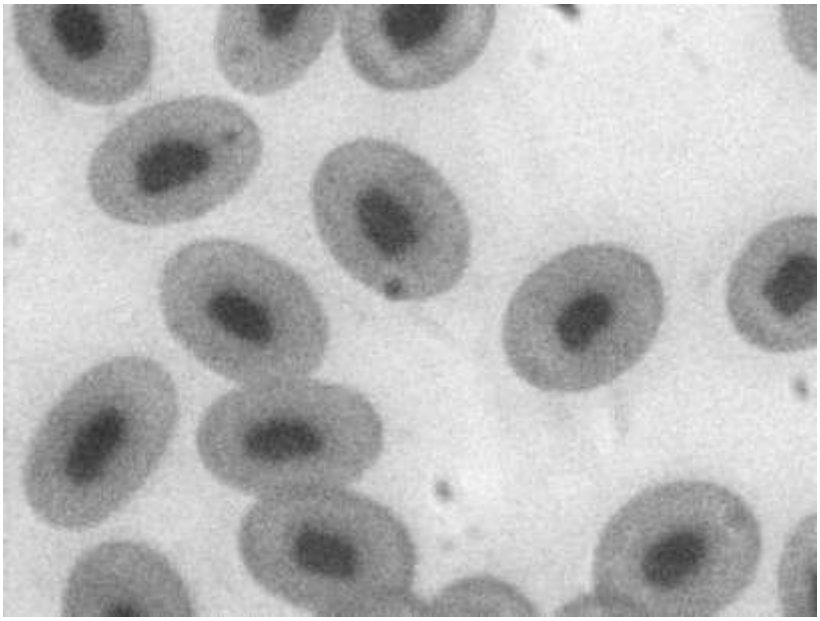

Figure 4.29: Bright field image of frog blood cell.

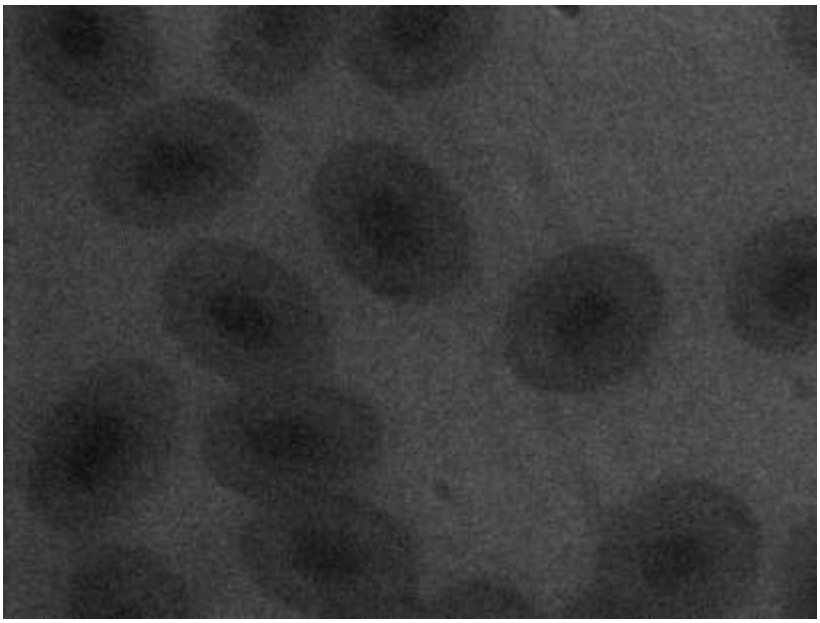

Figure 4.30: Dark field image of frog blood cell.

Figure 4.31: Retrieved quantitative phase estimate of frog blood cell.

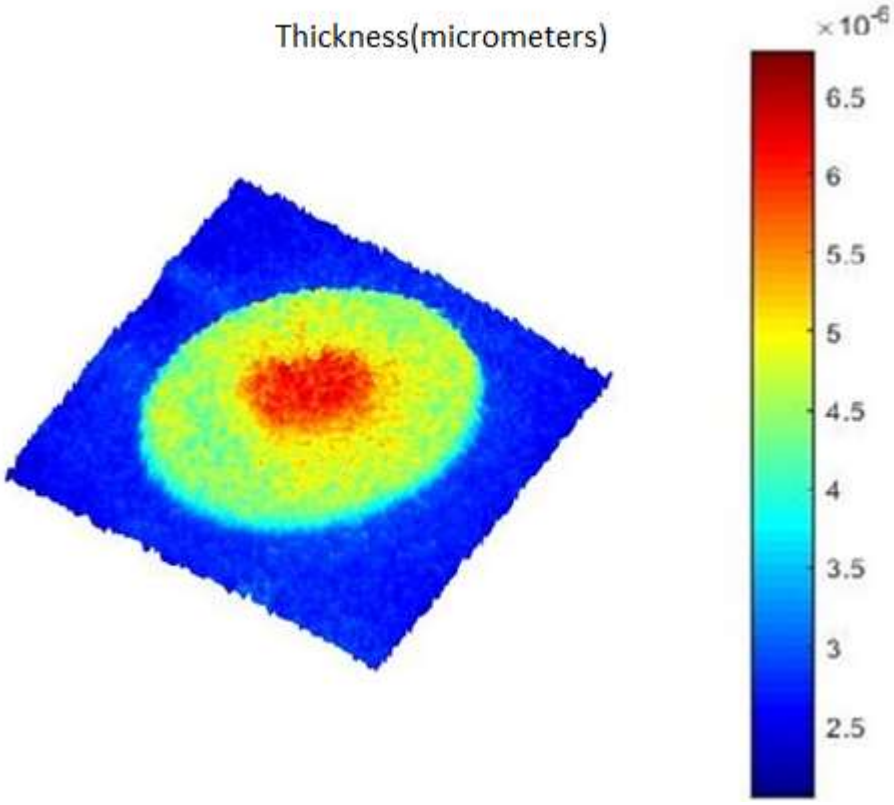

Figure 4.32: Retrieved quantitative phase estimate of frog blood cell.

Chapter 5
Summary and future work

In this work, we have developed and demonstrated a method to recover the object information behind the scattering media based on the speckle holography and two-point intensity correlation. The reconstruction of the object information from the speckle pattern originated from the scattering media is carried out by the application of Fourier fringe analysis of the complex coherence function obtained by spatially averaging speckle pattern under the assumption of spatial ergodicity. The experimental setup both single shot recovery and monitoring the flow behind the scattering medium is devised and demonstrated. The future work is aimed to develop this technique with appropriate changes in optical set-up to image the in vivo blood flow.

We have also developed and demonstrated a multi contrast microscopic platform for the successive acquisition of bright field, dark field and phase contrast modes. This diverse imaging capability is achieved by the sequential illumination of the specimen with different patterns on LED array. In addition, a novel algorithm for the quantitative phase reconstruction is also devised and the ability of the system to capture multicontrast images for different biological samples are demonstrated. The future work aims at the addition of new imaging modes like super resolution imaging in the multi contrast microscopic system with more sophisticated algorithms.

References

1. D. Gabor. A new microscope principle. *Nature*,161:777,1948.
2. Stroke, George W. “Coherent optics and holography.” Vol. 98. Academic Press Inc., New York, 1966.
3. Leith, Emmett N., and Juris Upatnieks. "Reconstructed Wavefronts and Communication Theory*." JOSA 52.10 (1962): 1123-1130.
4. Schnars, Ulf, and Werner Jüptner. "Direct recording of holograms by a CCD target and numerical reconstruction." Applied optics 33.2 (1994): 179-181.
5. Alfred Vogel and Vasan Venugopalan. Mechanisms of pulsed laser ablation of biological tissues. Chemical reviews, 103(2):577–644, February 2003.
6. Lihong V. Wang and Hsin-I Wu. Biomedical Optics: Principles and Imaging. John Wiley & Sons, 2012.
7. Vasilis Ntziachristos. Going deeper than microscopy: the optical imaging frontier in biology. Nature methods, 7(8):603–14, August 2010.
8. Yao, Gang, and Lihong Wang. "Propagation of polarized light in turbid media: simulated animation sequences." Optics Express 7.5 (2000): 198-203.
9. J M Schmitt, S H Xiang, and K M Yung. Speckle in optical coherence tomography. Journal of biomedical optics, 4(1):95–105, January 1999.
10. T. Loupas, W.N. McDicken, and P.L. Allan. An adaptive weighted median filter for speckle suppression in medical ultrasonic images. IEEE Transactionson Circuits and Systems, 36(1):129–135, January 1989
11. Jan Zizka, Alex Olwal, and Ramesh Raskar. Speckle Sense. In Proceedings of the 24th annual ACM symposium on User interface software and technology UIST ’11, page 489, New York, New York, USA, 2011. ACM Press.
12. Stroke, George W. “Coherent optics and holography.” Vol. 98. Academic Press Inc., New York, 1966.
13. Dainty, J. C. "I The statistics of speckle patterns." Progress in optics 14 (1977): 1-46
14. Goodman, Joseph W. Statistical optics. John Wiley & Sons, 2015.
15. Dainty, J. Christopher, ed. Laser speckle and related phenomena. Vol. 9. Springer Science & Business Media, 2013
16. R. Hanbury Brown and R. Q. Twiss, “Correlations between photons in two coherent beams of light,” Nature 177, 27–29 (1956).

17. M. Takeda, “Spatial stationarity of statistical optical fields for coherence holography and photon correlation holography,” Opt. Lett. 38(17), 3452–3455 (2013).
18. Singh, Rakesh Kumar, Raveendran Pillai Vasantha Kumari Vinu, and Megharaj Sharma Anandraj Sharma. "Retrieving complex coherence from two-point intensity correlation using holographic principle." Optical Engineering 53.10 (2014): 104102-104102.
19. Singh, Rakesh Kumar, Anandraj M. Sharma, and Bhargab Das. "Quantitative phase-contrast imaging through a scattering media." Optics letters 39.17 (2014): 5054-5057
20. J. Mertz, Introduction to Optical Microscopy (Roberts, 2010)
21. K. Summers and M. W. Kirschner, “Characteristics of the polar assembly and disassembly of microtubules observed in vitro by darkfield light microscopy,” J. Cell Biol. 83(1), 205–217 (1979).
22. S. Kudo, Y. Magariyama, and S. Aizawa, “Abrupt changes in flagellar rotation observed by laser dark-field microscopy,” Nature 346(6285), 677–680 (1990).
23. F. Zernike, “How I discovered phase contrast,” Science 121(3141), 345–349 (1955).
24. C. Burch and J. Stock, “Phase-contrast microscopy,” J. Sci. Instrum. 19(5), 71–75 (1942).
25. G. Nomarski, “Differential microinterferometer with polarized light,” Phys. Radium 16, 9–13 (1955).
26. E. D. Salmon and P. Tran, “High-resolution video-enhanced differential interference contrast light microscopy,”Methods Cell Biol. 72, 289–318 (2003).
27. G. Zheng, C. Kolner, and C. Yang, “Microscopy refocusing and dark-field imaging by using a simple LED array,” Optics Letters 36(20), pp. 3987–3989, 2011.
28. M. G. L. Gustafsson, Proc. Natl. Acad. Sci. USA 102,13081 (2005).
29. V. Poher, H. Zhang, G. Kennedy, C. Griffin, S. Oddos, E. Gu,D. Elson, M. Girkin, P. French, and M. Dawson, Opt.Express 15, 11196 (2007).
30. J. Wu, G. Zheng, Z. Li, and C. Yang, Opt. Lett. 36, 2179 (2011).
31. F. O. Fahrbach, P. Simon, and A. Rohrbach, Nat. Photon. 4,780 (2010).
32. L. Tian, J. Wang, L. Waller, Optics Letters, 39(5), 1326-1329 (2014).
33. A. B. Parthasarathy, K. K. Chu, T. N. Ford, and J. Mertz, Opt. Lett. 37, 4062 (2012).
34. M. R. Arnison, K. G. Larkin, C. J. R. Sheppard, N. I. Smith,and C. J. Cogswell, J. Microsc. 214, 7 (2004).